miR-802 Suppresses Acinar-to-Ductal Reprogramming During Early Pancreatitis and Pancreatic Carcinogenesis

Journal Article

Author(s):
Ge, Wenjie; Goga, Algera; He, Yuliang; Silva, Pamuditha N.; Hirt, Christian Kurt; Herrmanns, Karolin; Guccini, Ilaria; Godbersen, Svenja; Schwank, Gerald; Stoffel, Markus

Publication date:
2022-01

Permanent link:
https://doi.org/10.3929/ethz-b-000521369

Originally published in:
Gastroenterology 162(1), https://doi.org/10.1053/j.gastro.2021.09.029

Gastroenterology 2022;162:269–284

miR-802 Suppresses Acinar-to-Ductal Reprogramming During Early Pancreatitis and Pancreatic Carcinogenesis

Wenjie Ge,[1] Algera Goga,[1] Yuliang He,[2] Pamuditha N. Silva,[1] Christian Kurt Hirt,[1] Karolin Herrmanns,[1] Ilaria Guccini,[1] Svenja Godbersen,[1] Gerald Schwank,[3] and Markus Stoffel[1,4]

[1]*Institute of Molecular Health Sciences, ETH Zürich, Zürich, Switzerland;* [2]*Institute of Pharmaceutical Sciences, Swiss Federal Institute of Technology, Zürich, Switzerland;* [3]*Institute of Pharmacology and Toxicology, University of Zürich, Zürich, Switzerland; and* [4]*Medical Faculty, University of Zürich, Zürich, Switzerland*

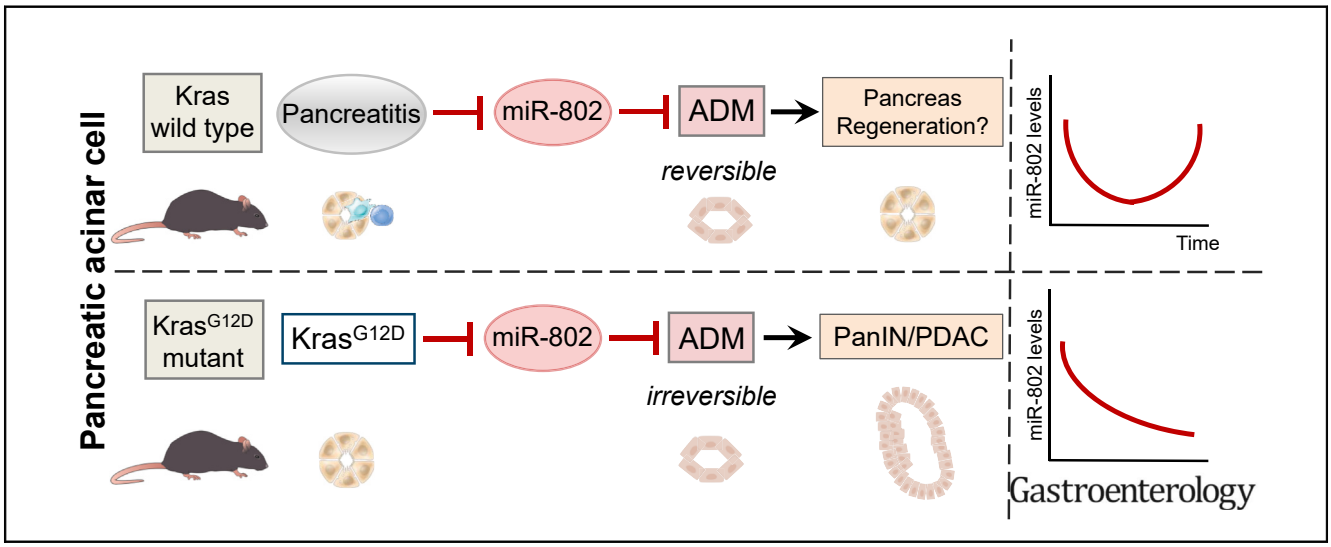

See editorial on page 48.

BACKGROUND & AIMS: Pancreatic ductal adenocarcinoma (PDAC) is a highly aggressive tumor that is almost uniformly lethal in humans. Activating mutations of KRAS are found in >90% of human PDACs and are sufficient to promote acinar-to-ductal metaplasia (ADM) during tumor initiation. The roles of miRNAs in oncogenic *Kras*-induced ADM are incompletely understood. **METHODS:** The *Ptf1a*$^{Cre/+}$ *LSL-Kras*$^{G12D/+}$ and *Ptf1a*$^{Cre/+}$ *LSL-Kras*$^{G12D/+}$ *LSL-p53R172H/*$^{+}$ and caerulein-induced acute pancreatitis mice models were used. *mir-802* was conditionally ablated in acinar cells to study the function of miR-802 in ADM. **RESULTS:** We show that miR-802 is a highly abundant and acinar-enriched pancreatic miRNA that is silenced during early stages of injury or oncogenic *Kras*^{G12D}-induced transformation. Genetic ablation of *mir-802* cooperates with *Kras*^{G12D} by promoting ADM formation. miR-802 deficiency results in de-repression of the miR-802 targets *Arhgef12*, *RhoA*, and *Sdc4*, activation of RhoA, and induction of the downstream RhoA effectors ROCK1, LIMK1, COFILIN1, and EZRIN, thereby increasing F-actin rearrangement. *mir-802* ablation also activates SOX9, resulting in augmented levels of ductal and attenuated expression of acinar identity genes. Consistently with these findings, we show that this miR-802–RhoA–F-actin network is activated in biopsies of pancreatic cancer patients and correlates with poor survival. **CONCLUSIONS:** We show miR-802 suppresses pancreatic cancer initiation by repressing oncogenic *Kras*-induced ADM. The role of miR-802 in ADM fills the gap in our understanding of oncogenic *Kras*-induced F-actin reorganization, acinar reprogramming, and PDAC initiation. Modulation of the miR-802–RhoA–F-actin network may be a new strategy to interfere with pancreatic carcinogenesis.

Keywords: Pancreatic Cancer; Pancreatitis; Micro-RNA.

Owing to the absence of measures that would facilitate the timely diagnosis at an early stage of pancreatic ductal adenocarcinoma (PDAC), patients with

Abbreviations used in this paper: **ADM, acinar-to-ductal metaplasia; CK19, cytokeratin 19; IB, immunoblot; IHC, immunohistochemistry; KC, *Ptf1a*$^{Cre/+}$ *Kras*$^{G12D/+}$; KPC, *Ptf1a*$^{Cre/+}$ *Kras*$^{G12D/+}$ *P53*$^{R172H/+}$; PanIN, pancreatic intraepithelial neoplasia; PDAC, pancreatic ductal adenocarcinoma; TCGA, The Cancer Genome Atlas.**

Most current article

0016-5085
https://doi.org/10.1053/j.gastro.2021.09.029

WHAT YOU NEED TO KNOW

BACKGROUND AND CONTEXT

Oncogenic *Kras*-induced acinar-to-ductal metaplasia (ADM) is the initiation step of pancreatic cancer. The role of miRNAs in the ADM process is poorly understood.

NEW FINDINGS

miR-802, a highly abundant and acinar-enriched pancreatic miRNA, is silenced in pancreatic injury or $Kras^{G12D}$-induced acinar reprogramming. Genetic ablation of *mir-802* results in de-repression of a miR-802 target network, leading to the activation of RhoA–F-actin rearrangement and SOX9, thus facilitating $Kras^{G12D}$-mediated ADM formation.

LIMITATIONS

Future studies should aim to clarify the role of phos-SOX9 (S181) in pancreatic cancer initiation.

IMPACT

miR-802 is a context-dependent and negative regulator of ADM by attenuating oncogenic *Kras*-mediated F-actin reorganization and acinar identity.

this disease are usually diagnosed at an advanced stage. Therefore, efforts to define the molecular mechanism that underlie the initiation of PDAC are highly relevant for early detection and options that enable early intervention.[1,2]

Mutations in the gene encoding KRAS have been reported to be present in more than 90% of human PDAC and found in more than 95% of the pre-cancerous pancreatic intraepithelial neoplasia (PanIN).[3] Consequently, the $Ptf1a^{Cre/+}$ $LSL\text{-}Kras^{G12D/+}$ mouse strain has been modeled to closely recapitulate pancreatic cancer initiation and progression in humans.[4]

Acinar cells are the dominant cell types of the pancreas. They exhibit high plasticity and can undergo a trans-differentiation process to a progenitor-like cell type with ductal characteristics, termed acinar-to-ductal metaplasia (ADM). ADM is critical for pancreas regeneration after injury and reversible once the injury is resolved. ADM also exhibits a tumorigenic potential, as ADM becomes irreversible in the presence of oncogenic *Kras* mutations in mice.[5] However, the molecular mechanisms and downstream targets of oncogenic *Kras* that regulate ADM are incompletely understood.

MicroRNAs (miRNAs) are small noncoding RNAs that function as posttranscriptional repressors of gene expression.[6] Inactivation of *dicer, mir-216a/b*, and *mir-217* in the pancreas leads to increased acinar cell plasticity and promotes $Kras^{G12D}$-induced ADM, but not PanIN, in KC mice,[7–9] indicating the presence of miRNA networks in the regulation of acinar identity and oncogenic *Kras*-mediated ADM. RNA-seq analysis of human PDAC revealed a striking down-regulation of miR-802.[10] Furthermore, we have previously demonstrated a role of miR-802 in differentiation and proliferation of the small intestine.[11] Therefore, in the present study, we investigated the expression and function of miR-802 in mice with $Kras^{G12D}$ and $Kras^{G12D}/Trp53^{R172H}$-driven PDAC, examined tumor initiation and progression, and identified an miR-802–regulated network that affects ADM through the regulation of the RhoA-Rock1 and Sox9 pathways. Finally, we relate our findings to miR-802 target gene engagement, gene expression, and patient survival in human PDAC.

Materials and Methods

In Vivo Animal Studies

All animal experiments were in accordance with institutional guidelines and approved by the Kantonale Veterinäramt Zürich. Mice were housed in a pathogen-free animal facility at the Institute of Molecular Systems Biology at the Swiss Federal Institute of Technology in Zurich. The animals were maintained in a temperature-controlled room (22°C), with humidity at 55% and on a 12 -hour light-dark cycle (lights on from 6 AM to 6 PM). Mice were fed a standard laboratory chow diet and water ad libitum, and the ages of the mice are indicated in the Figures. Both male and female mice were used in this study.

$LSL\text{-}Kras^{G12D}$, $Ptf1a^{Cre}$, $Ptf1a^{CreER}$, and $LSL\text{-}P53^{R172H}$ lines have been described before.[12–15] The $mir\text{-}802^{fl/fl}$ mice were generated by our laboratory.[11] All mice were maintained on a mixed background. The genotyping primers and representative genotyping results are described in the Supplementary Material. The $Ptf1a^{Cre/+}$ $Kras^{G12D/+}$ (KC) and $Ptf1a^{Cre/+}$ $Kras^{G12D/+}$ $P53^{R172H/+}$ (KPC) mice were monitored twice per week and tissues were collected when the mice lost more than 10% body weight within 1 week or exhibited symptoms like shaggy fur and hunched attitude.

For acute pancreatitis, 10–12-week-old WT and $mir\text{-}802^{KO}$ mice were induced by 8 intraperitoneal injections of caerulein, administered in 1-hour intervals on 2 consecutive days at a dose of 50 μg/kg body weight. Control mice received phosphate-buffered saline solution injection. The final day of caerulein injection was defined as day 0. Mice were killed at the indicated time points after the last injection.

Cell Cultures

AsPC-1, BxPC-3, SW1990, CFPAC-1, and Panc-10.05 were maintained in RPMI-1640 medium supplemented with 10% (v/v) fetal bovine serum (FBS) and 1% penicillin-streptomycin (P/S). Panc-1, 266-6, and HPAC were grown in DMEM with the same supplement. H6C7 was maintained in Keratinocyte-SFM (1×) following the manufacturer's instructions. 3D primary acinar explants were maintained in type I collagen and 3D culture medium (RPMI-1640 supplemented with 1% FBS, 1% P/S, 0.1 mg/mL trypsin inhibitors, 1 μg/mL dexamethasone). All cells were grown at 37°C in a humidified incubator with 5% CO_2.

Statistical Analysis

Data were analyzed with the use of GraphPad Prism 7.00. The mice survival data were analyzed by means of log-rank Mantel-Cox test. Tumor incidence frequency and metastasis potential were analyzed by Fisher's exact test. Data represent mean values ± SD from at least 3 independent experiments. Unpaired Student t test was used to compare between 2 groups. $P < 0.05$ was considered to be statistically significant.

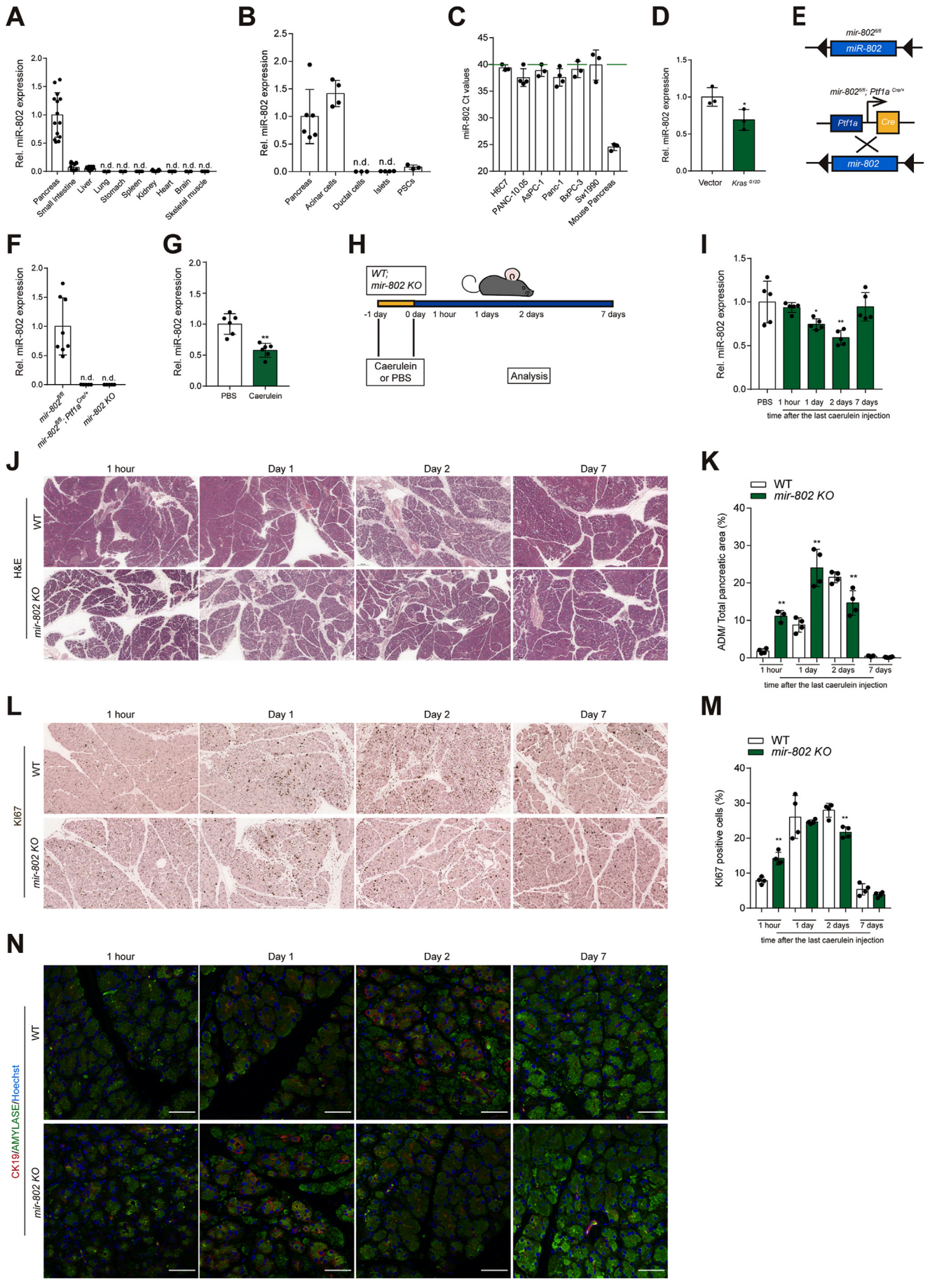
A
Rel. miR-802 expression
Pancreas
Small intestine
Liver
Lung
Stomach
Spleen
Kidney
Heart
Brain
Skeletal muscle
n.d.
B
Rel. miR-802 expression
Pancreas
Acinar cells
Ductal cells
Islets
PSCs
C
miR-802 Ct values
H6C7
PANC-10.05
AsPC-1
Panc-1
BxPC-3
Sw1990
Mouse Pancreas
D
Rel. miR-802 expression
Vector
Kras G12D
E
mir-802fl/fl
miR-802
mir-802fl/fl; Ptf1a Cre/+
Ptf1a
Cre
mir-802
F
Rel. miR-802 expression
mir-802fl/fl
mir-802fl/fl; Ptf1a Cre/+
mir-802 KO
G
Rel. miR-802 expression
PBS
Caerulein
H
WT;
mir-802 KO
-1 day
0 day
1 hour
1 days
2 days
7 days
Caerulein
or PBS
Analysis
I
Rel. miR-802 expression
PBS
1 hour
1 day
2 days
7 days
time after the last caerulein injection
J
1 hour
Day 1
Day 2
Day 7
H&E
WT
mir-802 KO
K
WT
mir-802 KO
ADM/ Total pancreatic area (%)
1 hour
1 day
2 days
7 days
time after the last caerulein injection
L
1 hour
Day 1
Day 2
Day 7
KI67
WT
mir-802 KO
M
WT
mir-802 KO
KI67 positive cells (%)
1 hour
1 day
2 days
7 days
time after the last caerulein injection
N
1 hour
Day 1
Day 2
Day 7
CK19/AMYLASE/Hoechst
WT
mir-802 KO

Results

miR-802 is Enriched in Acinar Cells and Decreased During Cell Transformation

Because cellular abundance of miRNAs is critical for their function, we analyzed miR-802 levels in a panel of C57BL/6 mouse tissues. miR-802 levels were highest in the pancreas (Ct 25.4 ± 1.2), with much lower expression in the jejunum, liver, and kidney (Figure 1*A*). miR-802 was enriched in acinar cells and barely detectable in ductal, islet, and stellate cells (Figure 1*B*). A quantitative analysis of miR-802 and other known acinar-enriched miRNAs[16] revealed miR-802 as one of the acinar-enriched miRNAs, with a copy number of ∼85,000 per cell (Supplementary Figure S1*A*). miR-802 levels were very low in the human pancreatic duct epithelial cell line H6C7 (Ct 39.4) and human PDAC cells (Figure 1*C*). Finally, miR-802 levels decreased in the mouse acinar cell line 266-6 on expression of $Kras^{G12D}$ (Figure 1*D* and Supplementary Figure S1*B*).

To study the function of miR-802 in the exocrine pancreas, we generated mice harboring floxed homozygous *mir-802* alleles (*mir-802*$^{fl/fl}$) and an acinar-specific *Cre* transgene (*Ptf1a-Cre*), or mice with global deletion of *mir-802* (named *mir-802*^{KO}) (Figure 1*E* and Supplementary Figure S1*C* to *E*). miR-802 levels were undetectable in the pancreas of *Ptf1a-Cre mir-802*$^{fl/fl}$ and *mir-802*^{KO} mice (Figure 1*F*), thereby confirming miR-802's restricted expression in acinar cells. Surprisingly, *Ptf1a-Cre miR-802*$^{fl/fl}$ and *mir-802*^{KO} mice exhibited normal pancreas mass, morphology, extracellular matrix, cell identity (CK19), and proliferation (KI-67) (Supplementary Figure S1*F* to *I*).

A key initiating step in both malignant transformation and injury of acinar cells is the transient formation of ADM and concomitant acinar cell proliferation.[17] We investigated whether miR-802 is dysregulated in the acute pancreatitis model and if this affects ADM formation. Treatment of 266-6 cells with caerulein, a cholecystokinin receptor agonist inducing acinar cell stress, reduced miR-802 expression (Figure 1*G*). Induction of acute pancreatitis by administration of caerulein in wild-type and *mir-802*^{KO} mice (Figure 1H),[4] resulted in a rapid decrease of miR-802 and increased ADM formation (Figure 1*I* and *J*). This inverse relationship was not observed for the pancreas-enriched miR-152 (Supplementary Figure S1*J*). Importantly, *mir-802*^{KO} mice showed increased ADM formation soon after the last caerulein injection (1 hour and 1 day) compared with control littermates (Figure 1*J* and 1*K*). The early increase in ADM formation in *mir-802*^{KO} mice was accompanied with increased KI67 staining, consistent with the transient increase in proliferation of metaplastic acinar cells[18] (Figure 1*L* and 1*M*). Acinar marker *Amy1a* was reduced, while the ductal marker *CK19* increased in *mir-802*^{KO} mice during the early phase of pancreatitis (Figure 1*N* and Supplementary Figure S1*K* and *L*). After 7 days, both mutant and wild-type pancreata showed normal morphology and normalization of differentiation markers (Figure 1*J* and *N*; Supplementary Figure S1*K* and *L*). These data demonstrate that miR-802 is highly expressed in differentiated acinar cells and that expression is readily down-regulated on acinar injury, thereby promoting ADM and acinar cell proliferation.

Ablation of mir-802 *in Acinar Cells Synergizes With* $Kras^{G12D}$ *to Accelerate Pancreatic Cancer Initiation*

To determine whether miR-802 is involved in oncogenic *Kras*-induced PDAC initiation, we crossed the *mir-802*$^{fl/fl}$mice with KC mice (named *mir-802*KC), which develop pancreatic tumors with long latency and display the spectrum of preneoplastic lesions observed in human PDAC[19] (Figure 2*A* and Supplementary Figure S2*A*). *mir-802* ablation was confirmed by qPCR (Supplementary Figure S2*B*). We studied KC and *mir-802*KC mice longitudinally and killed them when body weight loss was ≥10% or they showed disease symptoms. We found that 70% of *mir-802*KC mice developed PDAC, compared with 44.4% of KC mice (Figure 2*B*). Ablation of *mir-802* profoundly shortened the median survival of KC mice from 481 to 271 days (Figure 2*C*) and increased pancreas mass of 1-, 3-, and 6-month-old animals (Figure 2*D*), which was composed mostly of tumor at the last time point (Supplementary Figure S2*C*). Pancreatic miR-802 levels were dramatically decreased in 3- and 6-month-old KC mice compared with control littermates (Figure 2*E*), suggesting that miR-802 is important for *Kras*-induced transformation.

Figure 1. miR-802 is enriched in pancreatic acinar cells and silenced on transformation. (*A*) Relative miR-802 levels in indicated tissues of C57BL/6 mice (n = 4–18). Mean ± SD. n.d., not detectable. (*B*) Relative miR-802 levels in mouse pancreas and primary acinar, ductal, islet, and stellate cells (n = 6 in pancreas; n = 4 in acinar cells; n = 3 in ductal cells; n = 4 in islets; n = 3 in pancreatic stellate cells [PSCs]). (*C*) Ct values of miR-802 in H6C7, indicated pancreatic ductal adenocarcinoma cell lines and total pancreas of C57BL/6 mice (n = 3–4). The *green dashed line* indicates the detection threshold. (*D*) miR-802 levels in 266-6 cells transfected with 1 μg $Kras^{G12D}$ plasmid and related controls for 48 hours (n = 3). *$P < .05$. (*E*) Genetic strategy used to delete *mir-802* in the exocrine pancreas. (*F*) miR-802 measurements in pancreas of *mir-802*$^{fl/fl}$ (n = 8), *mir-802*$^{fl/fl}$ *Ptf1a*$^{Cre/+}$ (n = 5), and *mir-802*^{KO} (n = 5) mice. KO, knockout. (*G*) miR-802 levels in 266-6 cells treated with caerulein or phosphate-buffered saline solution (PBS) for 2 hours (n = 6). **$P < .01$. (*H*) Induction of acute pancreatitis in *mir-802*^{KO} and control mice. Mice were killed at the indicated time points after the last injection. (*I*) miR-802 levels in wild-type (WT) mice at indicated time points, after PBS injections for 7 days, or at indicated time points after the last caerulein injection (n = 5). *$P < .05$; **$P < .01$. (*J*) Hematoxylin and eosin (H&E) staining of pancreas sections described in (*H*). Scale bar = 200 μm. (*K*) Quantification of acinar-to-ductal metaplasia (ADM) area of the mice described in (*J*) (n = 4–5 WT mice; n = 3–4 *mir-802*^{KO} mice). **$P < .01$. (*L*) KI67 immunohistochemistry in pancreas sections described in (*J*). Scale bar = 50 μm. (*M*) Quantification of KI67-positive cells shown in (*L*) (n = 4). **$P < .01$. (*N*) Immunofluorescent staining of amylase, CK19, and Hoechst 33342 in pancreas sections described in (*J*). Scale bar = 50 μm.

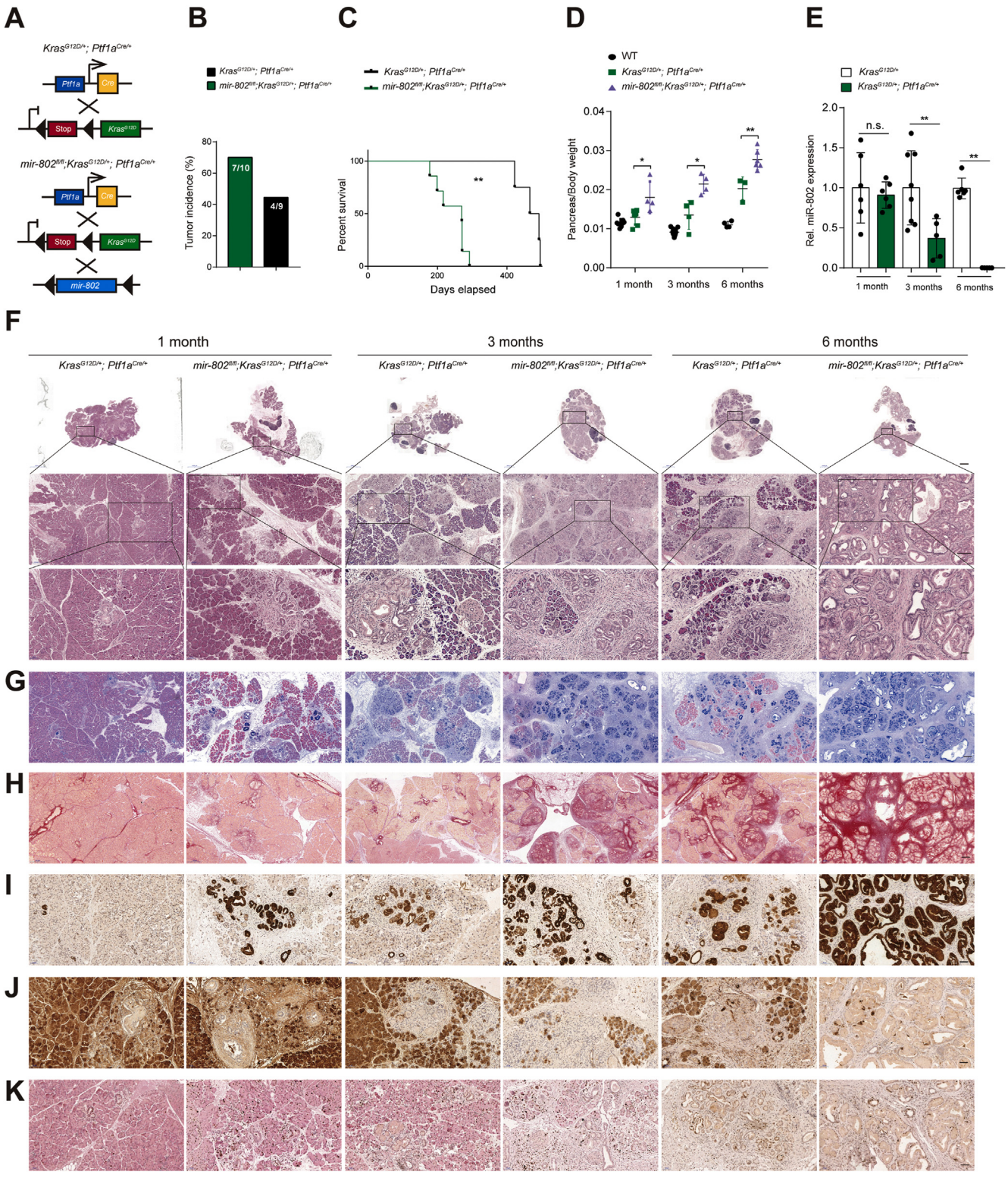

Figure 2. Ablation of *mir-802* in pancreatic acinar cells synergizes with *Kras*^{G12D} to accelerate cancer initiation. (*A*) Genetic strategy for acinar-specific ablation of *mir-802* and activation of *Kras.*^{G12D} (*B*) Tumor incidence rates in KC and *mir-802*KC mice. KC: n = 9; *mir-802*KC: n = 10. (*C*) Kaplan-Meier survival analysis of KC and *mir-802*KC mice. KC: n = 4; *mir-802*KC: n = 7. $^{**}P < .01$, log-rank test. (*D*) Pancreas/body weight ratio of 1-, 3-, and 6-month-old mice with indicated genotypes. Control: n = 4–11; KC: n = 3–7; *mir-802*KC: n = 4–6. Mean ± SD. $^{*}P < .05$; $^{**}P < .01$. (*E*) Pancreatic miR-802 levels from 1-, 3-, and 6-month-old mice with indicated genotypes. *Kras*^{G12D}: n = 6–8; KC: n = 5–6. $^{**}P < .01$; n.s., $P > 0.05$. (*F*) Hematoxylin and eosin, (*G*) Alcian blue and eosin, (*H*) Sirius red, (*I*) CK19 immunohistochemistry (IHC), (*J*) amylase IHC, and (*K*) KI67 IHC staining of pancreata from 1-, 3,- and 6-month-old animals with indicated genotypes. Scale bars: *F*: top row 2 mm, second row 200 μm, third row 50 μm); *G*, *H*: 200 μm; *I–K*: 50 μm.

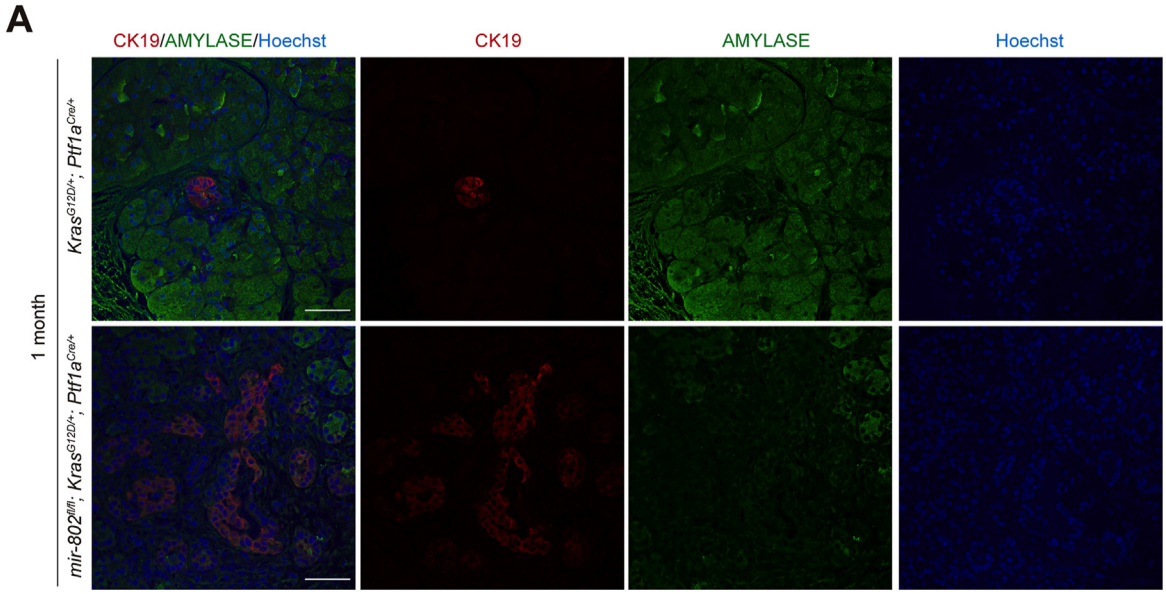
A
CK19/AMYLASE/Hoechst
CK19
AMYLASE
Hoechst
1 month
KrasG12D/+; Ptf1aCre/+
mir-802fl/fl; KrasG12D/+; Ptf1aCre/+

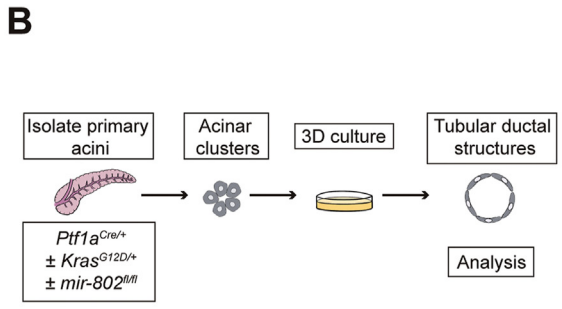
B
Isolate primary acini
Acinar clusters
3D culture
Tubular ductal structures
Analysis
Ptf1aCre/+
± KrasG12D/+
± mir-802fl/fl

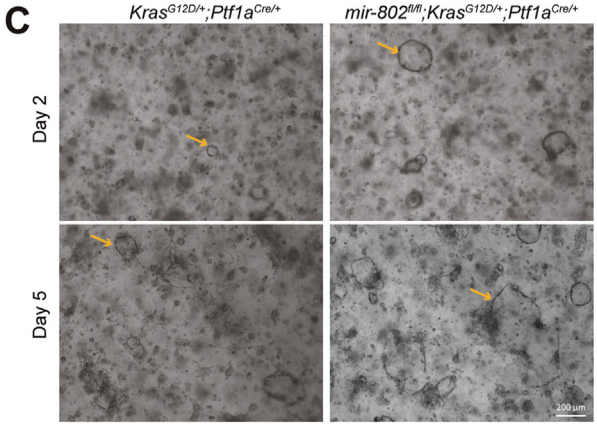
C
KrasG12D/+;Ptf1aCre/+
mir-802fl/fl;KrasG12D/+;Ptf1aCre/+
Day 2
Day 5
200 μm

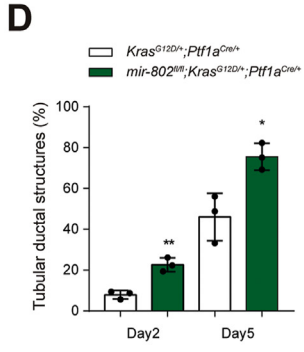
D
KrasG12D/+;Ptf1aCre/+
mir-802fl/fl;KrasG12D/+;Ptf1aCre/+
Tubular ductal structures (%)
Day2
Day5

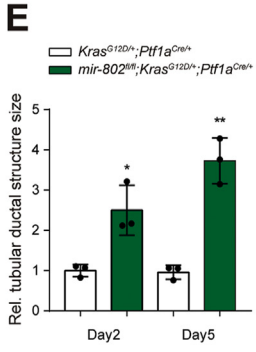
E
KrasG12D/+;Ptf1aCre/+
mir-802fl/fl;KrasG12D/+;Ptf1aCre/+
Rel. tubular ductal structure size
Day2
Day5

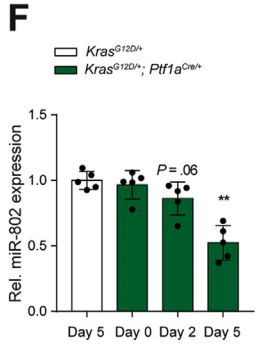
F
KrasG12D/+
KrasG12D/+; Ptf1aCre/+
Rel. miR-802 expression
P = .06
Day 5
Day 0
Day 2
Day 5

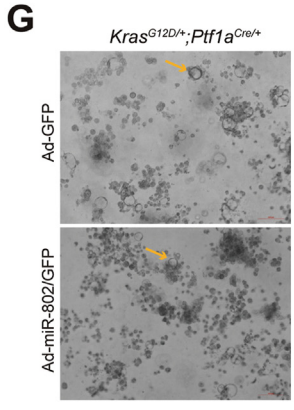
G
KrasG12D/+;Ptf1aCre/+
Ad-GFP
Ad-miR-802/GFP

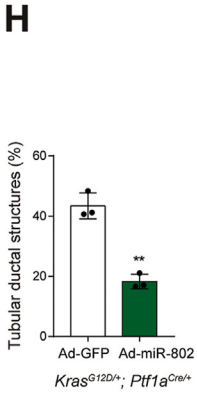
H
Tubular ductal structures (%)
Ad-GFP
Ad-miR-802
KrasG12D/+; Ptf1aCre/+

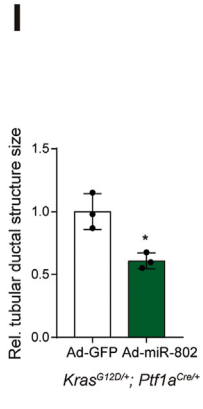
I
Rel. tubular ductal structure size
Ad-GFP
Ad-miR-802
KrasG12D/+; Ptf1aCre/+

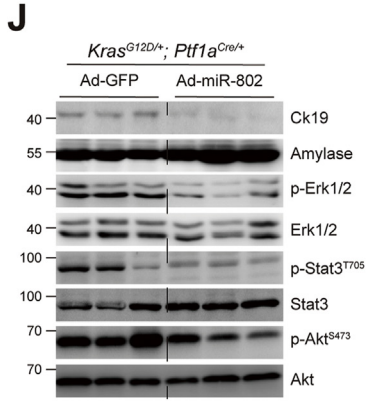
J
KrasG12D/+; Ptf1aCre/+
Ad-GFP
Ad-miR-802
Ck19
Amylase
p-Erk1/2
Erk1/2
p-Stat3T705
Stat3
p-AktS473
Akt

Histologic analysis of pancreatic sections from 1-, 3-, and 6-month-old mice show that the percentages of low-grade PanIN lesion in the KC mice were 0.4%, 1.3%, and 8.4%, respectively, compared with 3.0%, 8.2%, and 23.7% in *mir-802*KC pancreata (Figure 2*F* and *G* and Supplementary Figure S2*D* to *F*). Consistently, *mir-802* deletion in KC mice resulted in more collagen deposition (Figure 2*H* and Supplementary Figure S2*D* to *F*) and enhanced CK19-positive ductal lesions (Figure 2*I*), while the acinar area was decreased (Figure 2*J* and Supplementary Figure S2*D* to *F*). We also noted hyperplasia of ductal epithelial cells in 6-month-old *mir-802*KC mice (Figure 2*F*). Importantly, *mir-802*KC mice already show signs of cancer initiation at 1 month of age, as they have more ADM lesions (Figure 2*F* and Supplementary Figure S2*D*) and Ki67-positive cells (Figure 2*K* and Supplementary Figure S2*D*) compared with control mice. Furthermore, the PDAC-related STAT3, AKT, and ERK signaling pathways were up-regulated in *mir-802*KC mice (Supplementary Figure S2*G*). No differences in liver micro-metastasis were found between *mir-802*KC and KC mice (Supplementary Figure S2*H*).

Since human pancreatic cancer is caused by somatic *Kras* mutations in acinar cells during adulthood,[20] we crossed *mir-802*$^{fl/fl}$ mice with the *Ptf1a*$^{Cre\text{-}ERTM}$ line, allowing the tissue and time-specific ablation of *mir-802* in adult mice (Supplementary Figure S2*I* to *L*). Histologic analysis 4 weeks after *mir-802* deletion identified more ADM and Alcian blue–positive low-stage PanIN lesions in *mir-802*KC compared with KC mice (Supplementary Figure S2*M* to *P*). These results suggest that loss of *mir-802* in acinar cells cooperates with *Kras*^{G12D} to accelerate PDAC progression.

miR-802 Suppresses Pancreatic Carcinogenesis by Attenuating Kras*-Mediated ADM*

We next investigated if miR-802 regulates oncogenic *Kras*-mediated ADM. In support of the hematoxylin and eosin staining, we noticed increased CK19 and decreased amylase immunoreactivity in ADM lesions of *mir-802*KC mice (Figures 2*F* and 3*A*; Supplementary Figure S3*A*). To determine if miR-802 regulates ADM through a cell-autonomous effect, we used 3D-primary acinar cell cultures[21] and found ∼46% tubular-ductal cells derived from KC mice, whereas this fraction increased to 75.3% in *mir-802*KC animals on day 5. This phenotype was already apparent on day 2 (Figure 3*B* to *D*). Interestingly, *mir-802* ablation not only enhanced the formation but also led to an increase in the size of the "ductal structures" (Figure 3*E*). Similarly to observations in vivo, we found miR-802 levels decreased when "ductal structure" formation increased in 3D cultures from KC mice (Figure 3*F*). This phenotype could be reversed by infecting cells with an adenovirus expressing miR-802 (Supplementary Figure S3*B*). Re-expression of miR-802 reduced ADM numbers by 58% and ADM size by 40% (Figure 3*G* to *I*). Re-expression of miR-802 also reversed the identity of ADM cells and attenuated ERK, STAT3, and AKT signaling pathways (Figure 3*J*). These results indicated that miR-802 represses early neoplastic lesions by attenuating *Kras*-mediated ADM.

Arhgef12, RhoA, *and* Sdc4 *Are Direct Targets of miR-802 and Are Up-Regulated in* Kras^{G12D}*-Induced ADM*

To explore the mechanism by which miR-802 regulates ADM, we performed an integrated transcriptomic analysis of KC and *mir-802*KC pancreata with in silico miRNA target prediction algorithms. From RNA-seq, we found 5783 genes increased (adjusted log2 fold-change >0.4) in pancreata of *mir-802*KC compared with KC mice. An overlap of up-regulated transcripts in RNA-seq, and predicted miR-802 targets from TargetScan and miRDB revealed 24 transcripts with at least 1 evolutionarily conserved miR-802 binding site in the 3′UTR (Figure 4*A* and *B*). Metascape pathway analysis of these transcripts predicted that "cell junction assembly" and "PID_RhoA pathways" are enriched in *mir-802*KC pancreata (Figure 4*C*).[22] Consistently, analysis of 2786 genes that were significantly regulated (adjusted log2 fold-change >0.4; $P < 0.05$) in *mir-802*KC vs KC pancreata with the use of the Core Ingenuity Pathway Analysis showed enrichment for the RhoA-regulated canonic pathways (Figure 4*D*). These findings were supported by the de-repression of the miR-802 target RhoA in *mir-802*KC pancreata (Figure 4*B* and *H*; Supplementary Figure S4*A*). Consistent with increased RhoA expression, we identified higher levels of *Cdh11*, *Cdc42*, *Cfl2*, and *Rock1* transcripts (Figure 4*E* to *G*). These results established that loss of miR-802 in KC pancreata enhances RhoA expression and an associated network that is consistent with a more aggressive tumor phenotype.

RhoA is a critical member of Rho-GTPases, which regulate cytoskeleton dynamics by coordinating cell polarity, cell cycle progression, and migration.[23] Interestingly, we found that *mir-802*KC mice have increased mRNA levels of *RhoA*, RhoA upstream regulators *Cdh11* and *Sdc4*,[24,25] and RhoA

Figure 3. *mir-802* inactivation promotes oncogenic *Kras*-mediated pancreatic cancer by regulating acinar-to-ductal metaplasia (ADM). (*A*) Immunofluorescent staining of acinar cell marker amylase (Alexa 488), CK19 (Alexa 568), and Hoechst 33342 in pancreata of 1-month-old mice with indicated genotypes. Scale bar = 50 μm. (*B*) Scheme showing experiment design. (*C*) Brightfield images of primary acinar cell clusters after 2 and 5 days of collagen-based 3D cell culture. Arrows indicate ADM cells. Scale bar = 200 μm. (*D–E*) Quantification of tubular ductal structures and normalized size of primary acinar cell explants shown in (*C*) (n = 3). Mean ± SD. **P* < .05; ***P* < .01. (*F*) miR-802 levels in KC and control acinar explants after culture for indicated time (n = 5). ***P* < .01. (*G*) Brightfield images of acinar cell explants bearing the *Kras*^{G12D} mutation infected with adenovirus (Ad) expressing miR-802/green fluorescent protein (GFP) or control virus for 5 days. Arrows indicate ADM cells. Scale bar = 200 μm. (*H, I*) Quantification of tubular ductal structures and normalized size from the acinar cell explants shown in (*G*) (n = 3). **P* < .05; ***P* < .01. (*J*) Immunoblot analysis of whole-cell lysates from primary acinar cell explants described in (*G*).

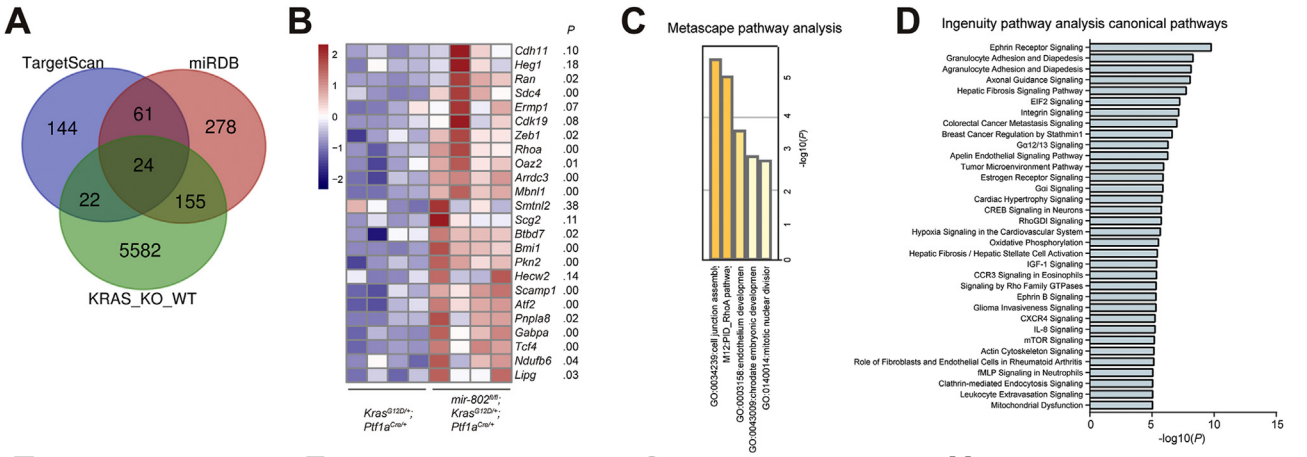

E

Signaling by Rho Family GTPases (IPA)

Gene symbol	log2 FC	P	Gene symbol	log2 FC	P
CDH26	5.17	.01	MYL9	0.96	.00
MYL4	2.83	.02	MRAS	0.94	.02
CDH17	2.69	.01	DES	0.94	.02
GNG4	2.46	.00	CFL2	0.90	.00
CDH8	2.46	.05	ITGAV	0.85	.00
CDH19	1.74	.01	VIM	0.81	.01
GNG11	1.53	.00	ACTR3	0.79	.00
ITGA8	1.52	.03	ARPC4	0.78	.01
NOX4	1.49	.00	ARHGEF3	0.78	.01
CDH11	1.49	.00	WIPF1	0.74	.01
GNG2	1.44	.00	PIK3C2A	0.72	.00
ARPC3	1.32	.00	RHOC	0.67	.04
PAK3	1.31	.00	PIK3CG	0.67	.02
MYLK	1.30	.71	RHOA	0.64	.00
GNG10	1.29	.00	CDC42EP3	0.63	.01
CDH3	1.17	.00	ITGB1	0.62	.00
ACTA2	1.16	.00	GNAI1	0.61	.01
GNAO1	1.15	.00	MYL6	0.61	.01
RHOJ	1.14	.00	RDX	0.60	.00
GNB4	1.11	.00	GNG12	0.56	.01
ITGB3	1.02	.00	MAPK8	0.50	.01
CDH5	1.02	.00	RAC1	0.50	.01
RHOB	1.01	.00	ARHGEF10	0.48	.04
CDH6	1.00	.03	ACTR2	0.47	.00
PIK3R3	0.98	.01	ROCK1	0.44	.02
Cdc42	0.98	.00	GNAI3	0.42	.01
ARPC5	0.97	.00	MYL12B	0.22	.36

F

Actin Cytoskeleton Signaling (IPA)

Gene symbol	log2 FC	P	Gene symbol	log2 FC	P
MYL4	2.83	.02	GSN	0.93	.00
Ins1	2.59	.00	VAV3	0.92	.01
FGF12	1.84	.03	CFL2	0.90	.00
FGF14	1.83	.02	FGF2	0.85	.02
RAP1B	1.71	.00	ITGAV	0.85	.00
F2R	1.68	.00	ACTR3	0.79	.00
ITGA8	1.52	.03	ABI2	0.79	.00
PDGFD	1.47	.00	ARPC4	0.78	.01
FGF1	1.40	.00	BRK1	0.76	.00
ARPC3	1.32	.00	PIK3C2A	0.72	.00
PAK3	1.31	.00	KRAS	0.67	.00
MYLK	1.30	.71	PIK3CG	0.67	.02
RAP1A	1.28	.00	RHOA	0.64	.00
CD14	1.22	.01	ARHGAP24	0.63	.01
PDGFC	1.18	.00	MYH11	0.63	.03
ACTA2	1.16	.00	ITGB1	0.62	.00
PPP1CB	1.11	.00	MYL6	0.61	.01
PFN2	1.07	.04	RDX	0.60	.00
ITGB3	1.02	.00	GNG12	0.56	.01
PIK3R3	0.98	.01	RALA	0.53	.00
ARPC5	0.97	.00	RAC1	0.50	.01
MYL9	0.96	.00	ACTR2	0.47	.00
MRAS	0.94	.02	ROCK1	0.44	.02
RRAS2	0.94	.00	HRAS	0.44	.02
			MYL12B	0.22	.36

G

Ephrin Receptor Signaling (IPA)

Gene symbol	log2 FC	P	Gene symbol	log2 FC	P
GNG4	2.46	.00	ITGAV	0.85	.00
VEGFC	2.00	.00	SDCBP	0.81	.00
RAP1B	1.71	.00	ACTR3	0.79	.00
GNG11	1.53	.00	ARPC4	0.78	.01
ITGA8	1.52	.03	WIPF1	0.74	.01
PDGFD	1.47	.00	EFNB2	0.72	.01
GNG2	1.44	.00	CREB1	0.71	.00
FGF1	1.40	.00	NCK1	0.69	.00
ARPC3	1.32	.00	KRAS	0.67	.00
PAK3	1.31	.00	PIK3CG	0.67	.02
GNG10	1.29	.00	EPHA4	0.67	.04
RAP1A	1.28	.00	RHOA	0.64	.00
EFNA1	1.22	.00	ITGB1	0.62	.00
PDGFC	1.18	.00	GNAI1	0.61	.01
GNAO1	1.15	.00	EFNB1	0.59	.02
GNB4	1.11	.00	GNG12	0.56	.01
ITGB3	1.02	.00	Wasl	0.54	.01
ABI1	1.02	.00	RALA	0.53	.00
ACP1	1.01	.00	RASA1	0.53	.00
SDC2	0.99	.00	FYN	0.52	.01
ANGPT1	0.99	.00	CXCL12	0.51	.02
ARPC5	0.97	.00	RAC1	0.50	.01
AKT3	0.95	.00	ACTR2	0.47	.00
MRAS	0.94	.02	ROCK1	0.44	.02
RRAS2	0.94	.00	HRAS	0.44	.02
CXCR4	0.91	.02	ATF2	0.43	.01
CFL2	0.90	.00	GNAI3	0.42	.01

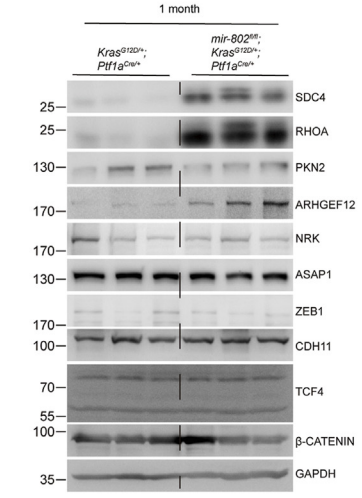

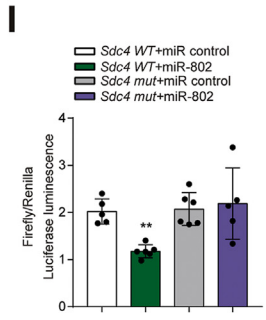

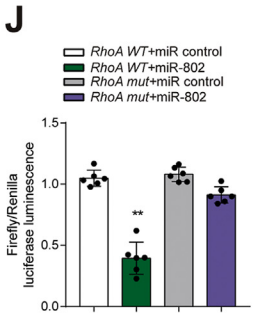

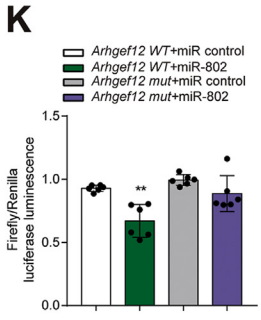

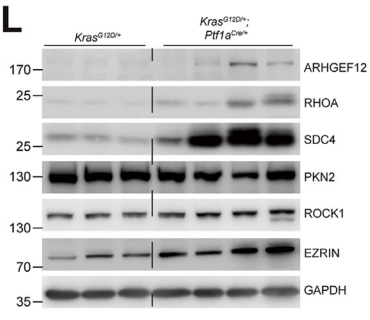

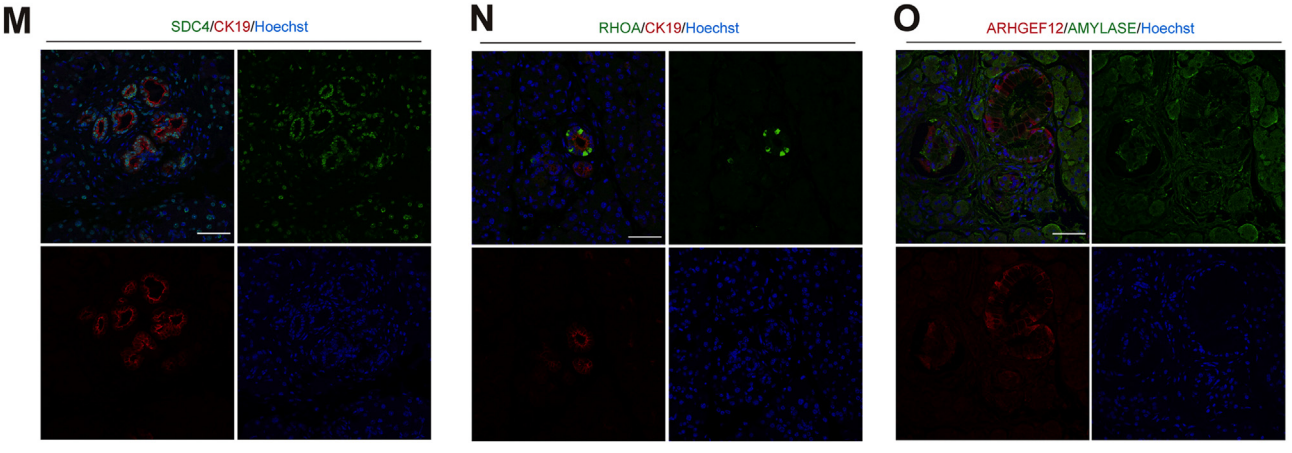

downstream effector *Pkn2*[26] (Figure 4*B*). The strong activation of RhoA and Sdc4 was confirmed by means of immunoblot analysis. Well known ADM regulators such as Zeb1, TCF4, and β-catenin remained unchanged (Figure 4*H* and Supplementary Figure S4*A*).[27,28]

To explore if other RhoA-related genes are regulated by miR-802, we searched the gene sets predicted by both TargetScan and miRDB (61 genes) (Figure 4*A*) and identified the RhoA guanine nucleotide exchange factor (GEF) *Arhgef12*, filament-actin binding protein *Asap1*, and filament-actin polymerization regulator *Nrk*.[29] Activation of Rho-GTPase is mainly controlled by GEFs, which activate Rho-GTPase by catalyzing the exchange of GDP for GTP.[23] Even though *Arhgef12* transcript levels were unchanged, we found increased ArhGEF12 protein levels in *mir-802*KC pancreata, indicating that miR-802 regulates *Arhgef12* translation rather than mRNA stability. No changes in NRK and ASAP1 protein levels were observed (Figure 4*H* and Supplementary Figure S4*A*). The de-repression of miR-802 targets RhoA, Sdc4, and ArhGEF12 was also discerned in the absence of oncogenic *Kras* in *mir-802*$^{fl/fl}$ *Ptf1a*$^{Cre/+}$ mice (Supplementary Figure S4*B* and *C*), indicating that their de-repression in *mir-802*^{KO} pancreata is not dependent on oncogenic stress. Finally, cross-species comparisons of the miRNA-binding sites in *Sdc4*, *RhoA*, and *Arhgef12* showed high evolutionary conservation (Supplementary Figure S4*D* to *F*) and pmiRGLO–dual luciferase reporter assays harboring wild-type or mutated 3′UTRs confirmed that they are direct miR-802 targets (Figure 4*I* to *K*; Supplementary Figure S4*G* to *I*).

To investigate the link of miR-802 targets and oncogenic *Kras*-induced ADM, we analyzed protein levels of ArhGEF12, RhoA, and Sdc4, together with the RhoA effectors Rock1[30] and Ezrin (EZR),[31] and found them to be up-regulated in KC compared with control mice (Figure 4*L* and Supplementary Figure S4*J*). Similarly, expression of ArhGEF12, RhoA, and Sdc4 was enriched specifically in ADM and PanIN lesions (Supplementary Figure S4*K* to *M*). Analysis of sections from 3-month-old KC pancreata revealed that ArhGEF12 and RhoA are located concisely in a subset of cells in ADM lesions, whereas Sdc4 was expressed in most ADM epithelial cells and a subset of stroma cells (Figure 4*M* to *O*). These results indicate that *Arhgef12*, *RhoA*, and *Sdc4* are direct targets of miR-802 and that their levels are increased in oncogenic *Kras*-induced ADM lesions.

miR-802 Attenuates Kras^{G12D}*-Induced ADM by Inhibiting F-Actin Reorganization and Sox9 Activity*

Rho-GTPase–dependent F-actin organization in acinar cells is required for cytoskeleton organization and acinar cell transformation, as inhibition of actin polymerization by cytochalasin D and latrunculin reduces the ADM formation.[32,33] Because RhoA is critical for F-actin organization and ADM formation,[34] we speculated that miR-802 controls *Kras*-induced ADM by influencing F-actin organization. Staining of pancreas sections from KC mice for F-actin with the use of phalloidin showed a strong intensity and redistribution in ADM, while it was restricted to the apical area in wild-type mice and in 3D cultures (Figure 5*A* and *B*), suggesting that the stability and distribution of F-actin are dysregulated in ADM lesions. Our RNA-seq analysis showed enriched gene sets in "increased organization of actin filaments" and "increased polymerization of actin filaments" (Supplementary Figure S5*A* and *B*). These results indicate that miR-802 regulates F-actin organization in the presence of oncogenic *Kras*.

To gain mechanistic insights in this process, we monitored the levels of RhoA-GTP with the use of the Rhotekin RBD-GST pull-down assay in KC and *mir-802*KC animals (Supplementary Figure S5*C*). RhoA-GTP levels increased ∼1.2-fold in *mir-802*KC-derived acinar cells, which also exhibited increased ArhGEF12, RhoA, and Sdc4 protein levels (Figure 5*C*). Furthermore, critical components of the "PID_RhoA pathway," including *Cyr61*, *Cdc42*, *RhoA*, *Ezr,* and *Rock1*, were increased in *mir-802*KC pancreata (Supplementary Figure S5*D*), thereby further strengthening the notion that *mir-802* deletion promotes RhoA activity in KC mice. Because RhoA controls F-actin polymerization mainly through the Rock1-Limk1-Cofilin pathway,[30] we explored whether this pathway is activated in *mir-802*KC pancreata and measured increased Rock1, Phos-Limk1, and Phos-Cofilin levels compared with KC mice (Figure 5*D* and Supplementary Figure S5*E*). Isolation of free globular- (G-actin) and F-actin from *mir-802*KC and KC pancreata by means of ultracentrifugation allowed us to measure a ∼22% increase in the F-actin ratio (Figure 5*E* and Supplementary Figure S5*F*). Conversely, miR-802 overexpression repressed ArhGEF12, RhoA, Sdc4 levels and the Rock1-Limk1-Cofilin pathway (Figure 5*F* and Supplementary Figure S5*G*) and reduced

Figure 4. *Arhgef12*, *RhoA*, and *Sdc4* are direct targets of miR-802 and are up-regulated in *Kras*^{G12D}-induced acinar-to-ductal metaplasia. (*A*) Venn diagram of up-regulated genes in 1-month-old *mir-802*KC pancreata compared to KC animals (log2 fold-change >0.4). (*B*) Heatmap showing the log2-transformed and scaled-normalized read counts of 24 genes from (*A*). (*C*) Metascape pathway analysis of 24 up-regulated potential miR-802 target genes. (*D*) Top canonic pathways from Ingenuity Pathway Analysis (IPA) of up-regulated genes in pancreata of 1-month-old *mir-802*KC compared with *KC* mice (n = 4 in each group; log2 fold-change >0.4; $P < 0.05$). (*E–G*) Gene expression analysis of indicated canonical pathways derived from IPA analysis shown in (*D*) (n = 4, normalized to KC). (*H*) Immunoblot analysis of pancreas lysates from 1-month-old KC and *mir-802*KC mice. (*I–K*) PmiRGLO dual-luciferase assay harboring wild-type (WT) and mutant (*mut*) miR-802 seed regions in the 3′UTR of indicated transcripts in Panc-1 cells (n = 5–6). $^{**}P < .01$. (*L*) Immunoblot analysis of pancreas whole-cell lysates from 1-month-old *Kras*$^{G12D/+}$ and *Kras*$^{G12D/+}$ *Ptf1a*$^{Cre/+}$mice. (*M–O*) Immunofluorescent staining of ArhGEF12/amylase, RhoA/CK19, and Sdc4/CK19 in pancreas sections of 3-month-old KC mice. Scale bar = 50 μm.

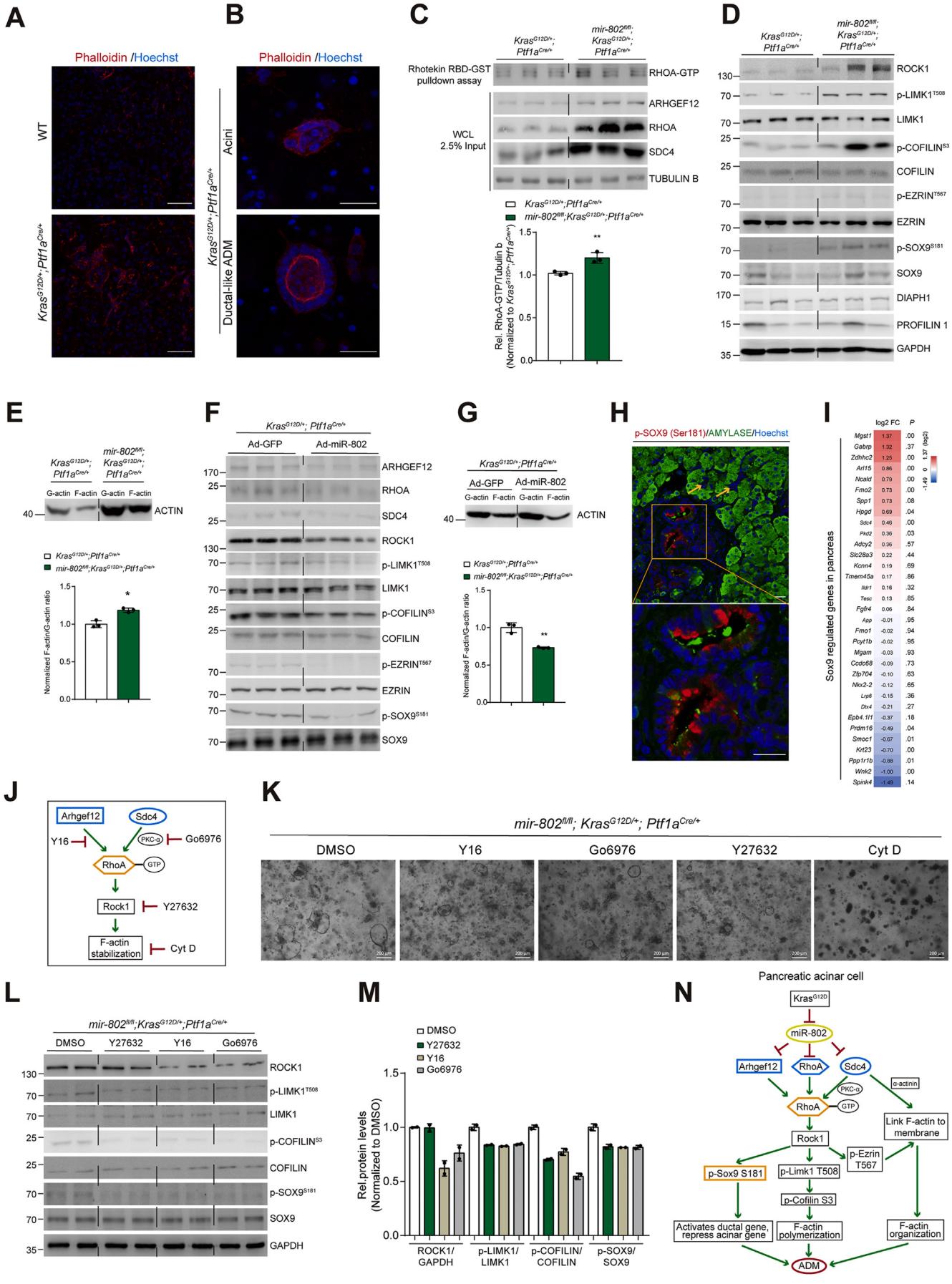
A
Phalloidin /Hoechst
WT
KrasG12D/+;Ptf1aCre/+
B
Phalloidin /Hoechst
KrasG12D/+;Ptf1aCre/+
Acini
Ductal-like ADM
C
KrasG12D/+; Ptf1aCre/+
mir-802fl/fl; KrasG12D/+; Ptf1aCre/+
Rhotekin RBD-GST pulldown assay
RHOA-GTP
ARHGEF12
RHOA
SDC4
TUBULIN B
WCL 2.5% Input
Rel. RhoA-GTP/Tubulin b (Normalized to KrasG12D/+;Ptf1aCre/+)
D
ROCK1
p-LIMK1T508
LIMK1
p-COFILINS3
COFILIN
p-EZRINT567
EZRIN
p-SOX9S181
SOX9
DIAPH1
PROFILIN 1
GAPDH
E
G-actin F-actin G-actin F-actin
ACTIN
Normalized F-actin/G-actin ratio
F
Ad-GFP
Ad-miR-802
ARHGEF12
RHOA
SDC4
ROCK1
p-LIMK1T508
LIMK1
p-COFILINS3
COFILIN
p-EZRINT567
EZRIN
p-SOX9S181
SOX9
G
Ad-GFP
Ad-miR-802
G-actin F-actin G-actin F-actin
ACTIN
Normalized F-actin/G-actin ratio
H
p-SOX9 (Ser181)/AMYLASE/Hoechst
I
log2 FC
P
Sox9 regulated genes in pancreas
Mgst1 1.37 .00
Gabrp 1.32 .37
Zdhhc2 1.25 .00
Arl15 0.86 .00
Ncald 0.79 .00
Fmo2 0.73 .00
Spp1 0.73 .08
Hpgd 0.69 .04
Sdc4 0.46 .00
Pkd2 0.36 .03
Adcy2 0.36 .57
Slc28a3 0.22 .44
Kcnn4 0.19 .69
Tmem45a 0.17 .86
Ildr1 0.16 .32
Tesc 0.13 .85
Fgfr4 0.06 .84
App -0.01 .95
Fmo1 -0.02 .94
Pcyt1b -0.02 .95
Mgam -0.03 .93
Ccdc68 -0.09 .73
Zfp704 -0.10 .63
Nkx2-2 -0.12 .65
Lrp6 -0.15 .36
Dtx4 -0.21 .27
Epb4.1l1 -0.37 .18
Prdm16 -0.49 .04
Smoc1 -0.67 .01
Krt23 -0.70 .00
Ppp1r1b -0.88 .01
Wnk2 -1.00 .00
Spink4 -1.45 .14
J
Arhgef12
Sdc4
Y16
PKC-α
Go6976
RhoA
GTP
Rock1
Y27632
F-actin stabilization
Cyt D
K
mir-802fl/fl; KrasG12D/+; Ptf1aCre/+
DMSO
Y16
Go6976
Y27632
Cyt D
L
mir-802fl/fl;KrasG12D/+;Ptf1aCre/+
DMSO
Y27632
Y16
Go6976
ROCK1
p-LIMK1T508
LIMK1
p-COFILINS3
COFILIN
p-SOX9S181
SOX9
GAPDH
M
DMSO
Y27632
Y16
Go6976
Rel.protein levels (Normalized to DMSO)
ROCK1/ GAPDH
p-LIMK1/ LIMK1
p-COFILIN/ COFILIN
p-SOX9/ SOX9
N
Pancreatic acinar cell
KrasG12D
miR-802
Arhgef12
RhoA
Sdc4
PKC-α
α-actinin
RhoA
GTP
Link F-actin to membrane
Rock1
p-Ezrin T567
p-Sox9 S181
p-Limk1 T508
p-Cofilin S3
Activates ductal gene, repress acinar gene
F-actin polymerization
F-actin organization
ADM

the F-actin ratio (Figure 5*G* and Supplementary Figure S5*H*) in 3D cultures, demonstrating that miR-802 controls F-actin stability in *Kras*^{G12D}-transformed acinar cells. In contrast, Rock1 downstream effectors Diapha1 and Profilin1, which are important for F-actin nucleation, were not deregulated (Figure 5*D* and Supplementary Figure S5*E*),[35] indicating that miR-802 affects F-actin polymerization rather than nucleation in KC animals. Finally, the expression of Phos-Ezrin and Sdc4, linking F-actin to the cell membrane directly or through α-actinin,[36,37] was also regulated by miR-802 (Figure 5*D* and *F*; Supplementary Figure S5*E* and *G*). These data show that miR-802 also influences the distribution of F-actin in KC mice through its action on Ezrin and Sdc4.

Rock1 directly phosphorylates Sox9 at Ser(181),[38] which is a critical transcriptional factor in ductal and centroacinar cells and responsible for ADM.[4] We explored if Sox9 and Phos-Sox9 are regulated by miR-802 in KC mice and primary acinar explants and found similar Sox9 levels; however, expression of Phos-Sox9 was negatively regulated by miR-802 (Figure 5*D* and 5*F*; Supplementary Figure S5*E* and *G*). Immunofluorescence staining showed that Phos-Sox9 was located strictly within ADM lesions and not in ductal cells (Figure 5*H*), supporting an active role in oncogenic *Kras*-induced ADM. This finding is supported by increased levels of SOX9 targets *Pkd2* and *Spp1*, both engaged in the maintenance of ductal cell identity,[39] and reduced expression of *the* acinar cell identity markers *Bhlha15* and *Rbpjl* in *mir-802*KC mice (Figure 5*I* and Supplementary Figure S5*I*).

Finally, we explored if *mir-802* ablation promotes ADM through regulation of the RhoA–Rock1–F-actin pathway by treating primary acinar explants derived from *mir-802*KC mice with specific inhibitors[24,30,32,40] (Figure 5*J*). The ADM-promoting effect of *mir-802* ablation was significantly repressed by all inhibitors, with strongest outcomes after cytochalasin D treatment (Figure 5*K* and Supplementary Figure S5*J* and *K*). The inhibition of the Rock1-Limk1-Cofilin1 pathway and Phos-Sox9 levels under these conditions was confirmed by immunoblot analysis (Figure 5*L* and *M*). Together, these results establish that miR-802 ablation activates the RhoA–Rock1–F-actin network, enhances Sox9 activity through phosphorylation, and thereby contributes to the repression of an acinar gene signature, thus promoting oncogenic *Kras*-induced ADM (Figure 5*N*).

Ablation of mir-802 *Accelerates the Development of PDAC in* LSL-Kras^{G12D} LSL-Trp53$^{R172H/+}$ Ptf1a$^{Cre/+}$ *(KPC) Mice*

See Supplementary Text and Supplementary Figures S6 and S7.

Increased Expression of miR-802 Targets Correlates With Poor Survival in PDAC Patients

To investigate the effect of miR-802 re-expression we monitored the expression in a panel of human PDAC cell lines and found increased protein levels of ArhGEF12, RhoA, Sdc4, other regulators of F-actin dynamics, and Sox9 compared with H6C7 cells (Figure 6*A*). Transfection of CFPAC-1 and Panc-1 cells with miR-802 mimics decreased active RhoA levels (Figure 6*B* and Supplementary Figure S8*A*), repressed miR-802 targets and downstream effectors (Figure 6*C* and *D*; Supplementary Figure S8*B* and *C*), reduced the F-actin/G-actin ratio, and affected the distribution of F-actin compared with scramble controls (Figure 6*E* and *F*; Supplementary Figure S8*D* and *E*). We also asked if miR-802 overexpression could be beneficial for the treatment of PDAC; however, human PDAC cells retained their viability, ductal identity, and oncofetal pathways (Supplementary Figure S8*F* to *I*). Patient-derived PDAC organoids also showed little effect on viability and morphology (Supplementary Figure S8*J* to *L*). These results reveal that miR-802 re-expression is insufficient to reverse the phenotype of established PDAC cells.

Finally, we investigated the relevance of miR-802 targets in human PDAC with the use of 2 cohorts of 178 PDAC and 167 normal pancreatic tissue datasets from The Cancer Genome Atlas (TCGA) and the Genotype-Tissue Expression (GTEx) project, respectively.[41] We discovered a significant enrichment of de-repressed miR-802 targets *Arhgef12*, *RhoA, Sdc4*, *Zeb1*, and *Tcf4* in biopsies of PDAC compared with normal pancreatic tissue (Figure 6*G* and Supplementary Figure S8*M*). Moreover, critical regulators affecting F-actin organization (ie, *Cfl1, Rock1*, *Limk1*, and

Figure 5. miR-802 attenuates *Kras*^{G12D}-induced acinar-to-ductal metaplasia (ADM) by inhibiting RhoA-dependent F-actin reorganization and Sox9 activity. (*A*, *B*) Phalloidin-TRITC and Hoechst 33342 staining in pancreatic sections from (*A*) 3-month-old wild-type (WT) and KC mice and in (*B*) 3D acinar explants bearing the *Kras*^{G12D} mutation. Scale bar = 50 μm. (*C*) Rhotekin RBD-GST pull-down and whole-cell lysate (WCL) analysis of freshly isolated acinar cells of 1-month-old KC and *mir-802*KC mice. Bar graph represents the relative quantification of RhoA-GTP levels (n = 3). Mean ± SD. $^{**}P < .01$. (*D*) Immunoblot (IB) of pancreas WCL from 1-month-old KC and *mir-802*KC mice. (*E*) F-actin/G-actin levels in freshly isolated acinar WCL from 1-month-old KC and *mir-802*KC mice. Bar graph indicates the quantification of F-actin/G-actin ratio (n = 3). $^{*}P < .05$. (*F*) IB of WCL from 3D primary acinar explants infected with adenovirus (Ad) expressing miR-802 or control for 5 days. (*G*) F-actin/G-actin levels in 3D acinar explants described in (*F*). Bar graph indicates the quantification of F-actin/G-actin ratio (n = 3). $^{**}P < .01$. (*H*) Immunofluorescent staining of Phos-Sox9 (S181)/amylase in the pancreas sections of 3-month-old KC mice. *Arrows* indicate ductal cells. Scale bar = 50 μm. (*I*) Gene expression of potential Sox9-regulated genes in pancreas (n = 4, normalized to KC mice). (*J*) Scheme showing targets of the indicated chemical inhibitors. (*K*) Brightfield image analysis of acinar cell explants isolated from *mir-802*KC mice, treated with DMSO, Y16 (50 μmol/L), Go6976 (1 μmol/L), Y27632 (10 μmol/L), and Cyt D (2 μmol/L) for 5 days. Scale bar = 200 μm. (*L*) IB of WCL from 3D acinar explants described in (*K*). (*M*) Quantification of the IB shown in (*L*) (n = 2). (*N*) Model illustrating how miR-802 controls ADM by repressing RhoA-dependent F-actin rearrangement and Phos-Sox9 levels in the presence of *Kras*^{G12D}.

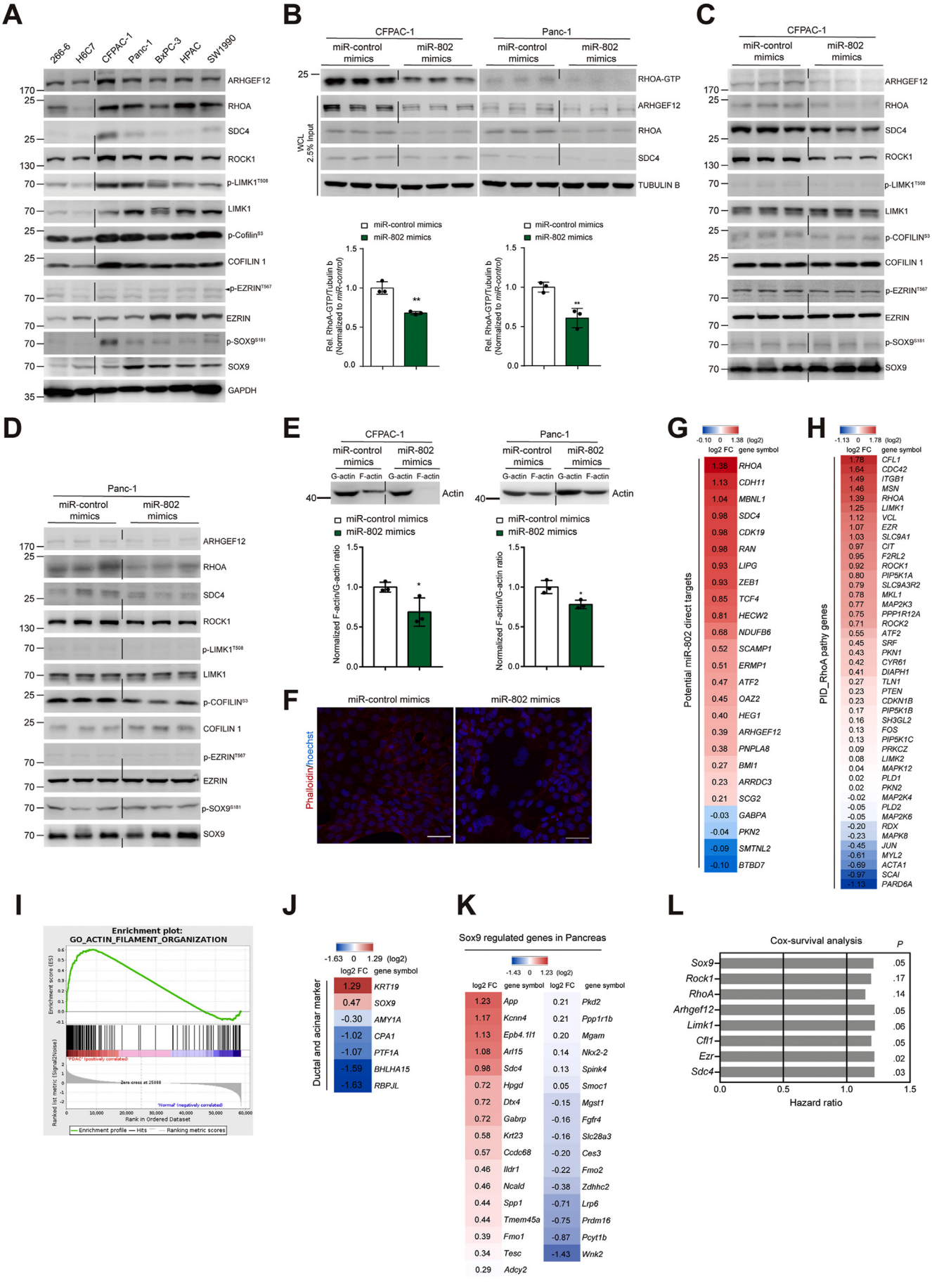
A
266-6
H6C7
CFPAC-1
Panc-1
BxPC-3
HPAC
SW1990
ARHGEF12
RHOA
SDC4
ROCK1
p-LIMK1T508
LIMK1
p-CofilinS3
COFILIN 1
p-EZRINT567
EZRIN
p-SOX9S181
SOX9
GAPDH
B
CFPAC-1
Panc-1
miR-control mimics
miR-802 mimics
RHOA-GTP
ARHGEF12
RHOA
SDC4
TUBULIN B
WCL 2.5% Input
Rel. RhoA-GTP/Tubulin b (Normalized to miR-control)
C
CFPAC-1
D
Panc-1
E
G-actin
F-actin
Actin
Normalized F-actin/G-actin ratio
F
Phalloidin/hoechst
G
Potential miR-802 direct targets
log2 FC
gene symbol
RHOA
CDH11
MBNL1
SDC4
CDK19
RAN
LIPG
ZEB1
TCF4
HECW2
NDUFB6
SCAMP1
ERMP1
ATF2
OAZ2
HEG1
ARHGEF12
PNPLA8
BMI1
ARRDC3
SCG2
GABPA
PKN2
SMTNL2
BTBD7
H
PID_RhoA pathy genes
CFL1
CDC42
ITGB1
MSN
RHOA
LIMK1
VCL
EZR
SLC9A1
CIT
F2RL2
ROCK1
PIP5K1A
SLC9A3R2
MKL1
MAP2K3
PPP1R12A
ROCK2
ATF2
SRF
PKN1
CYR61
DIAPH1
TLN1
PTEN
CDKN1B
PIP5K1B
SH3GL2
FOS
PIP5K1C
PRKCZ
LIMK2
MAPK12
PLD1
PKN2
MAP2K4
PLD2
MAP2K6
RDX
MAPK8
JUN
MYL2
ACTA1
SCAI
PARD6A
I
Enrichment plot:
GO_ACTIN_FILAMENT_ORGANIZATION
Enrichment score (ES)
Ranked list metric (Signal2Noise)
Rank in Ordered Dataset
Enrichment profile
Hits
Ranking metric scores
J
Ductal and acinar marker
KRT19
SOX9
AMY1A
CPA1
PTF1A
BHLHA15
RBPJL
K
Sox9 regulated genes in Pancreas
App
Kcnn4
Epb4.1l1
Arl15
Sdc4
Hpgd
Dtx4
Gabrp
Krt23
Ccdc68
Ildr1
Ncald
Spp1
Tmem45a
Fmo1
Tesc
Adcy2
Pkd2
Ppp1r1b
Mgam
Nkx2-2
Spink4
Smoc1
Mgst1
Fgfr4
Slc28a3
Ces3
Fmo2
Zdhhc2
Lrp6
Prdm16
Pcyt1b
Wnk2
L
Cox-survival analysis
P
Sox9
Rock1
RhoA
Arhgef12
Limk1
Cfl1
Ezr
Sdc4
Hazard ratio

Ezr) and other known RhoA effectors (*Msn*, *Cdc42*, *Vcl*) of the "PID_RhoA pathway" were overrepresented in patients' samples (Figure 6*H*).[42] These findings were further supported in a gene set enrichment analysis of TGCA patient sequencing data showing that the "Actin filament organization pathway" is strongly augmented in PDAC patients (Figure 6*I*). Specifically, the miR-802–regulated *RhoA*, *Ezr*, and the other known F-actin regulators involved in oncogenic *Kras*-induced ADM (ie, *Arpc2*, *Rac1*) were de-regulated in patients[32,43] (Supplementary Figure S8*N*). Sox9 activity may also be activated in PDAC patients, as revealed by the expression of pancreatic epithelial cell markers and reported Sox9-regulated genes (Figure 6*J* and *K*).[39] Consistently with our mouse data, we found that ArhGEF12, RhoA, and Sdc4 were also de-repressed in human biopsies of ADM, PanIN, and advanced PDAC lesions (Supplementary Figure S8*O* to *Q*). Importantly, a Cox proportional hazards survival analysis revealed that increased expression of *ARHGEF12*, *SDC4*, and downstream RhoA effectors (*Cfl1*, *Ezr*) correlated with poor survival of patients (Figure 6*L*).

Discussion

Activating *Kras* mutations represent the signature event in PDAC that drives PDAC initiation and progression. Although several downstream genes of oncogenic *Kras* have been found to mediate these processes, the role of miRNAs has not been thoroughly studied. Several studies indicate an important role of miRNAs in the regulation of ADM. Inactivation of *dicer* in the mouse pancreas results in increased ADM formation but animals do not develop more PanIN lesions compared with KC mice.[8] Inactivation of some highly expressed pancreatic miRNAs has been shown to enhance or repress PDAC development: Whereas *miR-216a/b* and *miR-217*–restricted deletion in acinar cells promotes ADM but has no influence on PDAC progression,[9] ablation of the *mir-181ab1* cluster in KC animals inhibits tumor initiation and progression.[44] These phenotypes highlight a highly complex miRNA network consisting of positive and negative miRNA regulators that influence PDAC initiation and progression. Our study shows that *mir-802* ablation in KC mice exhibit not only more ADM but also enhance PDAC progression, thereby underscoring an important role of miR-802 in pancreatic cancer development.

A fundamental question pertains to the physiological role of a conserved and highly expressed miR-802 that is dispensable for organ development and acinar cell differentiation. Our data suggest that miR-802 regulates the early stages of pancreas regeneration. During acute pancreatitis, ADM of acinar cells provides critical means for animals to maintain pancreas mass after injury.[5] Our data suggest that miR-802 is a negative regulator of ADM and acinar cell proliferation. Upon injury, miR-802 levels decrease, leading to a transient enhancement of a metaplastic process and resulting in ADM formation and acinar cell proliferation, thereby promoting the restoration of tissue homeostasis.

The most striking effect of *mir-802* ablation was observed in 2 pancreatic cancer models (KC and KPC), in which *mir-802* inactivation shortened the overall survival of both models. Genetic ablation of *mir-802* had an impressive tumor-promoting effect in KC mice, with an increase in ADM lesions already in 1-month-old mice, suggesting an inhibitory role of miR-802 during initial metaplasia. Moreover, the repressive effect of miR-802 on ADM could also readily be observed in primary acinar explants, supporting the notion that miR-802 suppresses pancreatic carcinogenesis. Conversely, miR-802 ectopic expression in human PDAC cells did not affect proliferation, viability, and cell identity, indicating that miR-802 has limited impact on advanced PDAC.

To elucidate the mechanism by which miR-802 protects against early stages of pancreatic cancer development we identified 3 direct and conserved miR-802 targets: 1) *RhoA*, one of the most important members of Rho-GTPase, 2) its GEF, *Arhgef12*, and 3) RhoA upstream regulator *Sdc4*. All of these targets affect RhoA activity. De-repression of ArhGEF12, RhoA, and Sdc4 in the pancreata of KC mice lacking *mir-802* leads to RhoA activation. Furthermore, these proteins are located in ADM and PanIN lesions of both mice and patients. These results place miR-802 downstream of oncogenic *Kras* and upstream of RhoA, ArhGEF12, and Sdc4.

Whereas high RhoA activity has been reported in a subset of pancreatic tumor cells in vivo,[45] Rho-GTPases are rarely mutated in human tumors, and analysis of the data set from TCGA did not identify oncogenic or amplification mutations in these genes.[46] However, expression analysis of this data set revealed that the mRNA levels of *RhoA*, *Arhgef12*, and *Sdc4* are increased and correlated with reduced survival in human PDAC. Our findings therefore offer a mechanistic explanation by which increased RhoA activity in PDAC is in part mediated by post-transcriptional regulation through silencing of miR-802 and de-repression of *Arhgef12*, *RhoA*, and *Sdc4*.

Figure 6. Elevated expression of miR-802 targets correlates with poor survival in pancreatic ductal adenocarcinoma (PDAC) patients. (*A*) IB of WCL from indicated cell lines. (*B*) Rhotekin RBD-GST pulldown and WCL analysis from CFPAC-1 and Panc-1 cells transfected with scrambled control or miR-802 mimics. Bar graph represents the quantification of RhoA-GTP levels (n = 3). Mean ± SD. $^{**}P < .01$. (*C*, *D*) IB of WCL from CFPAC-1 and Panc-1 cells described in (*B*). (*E*) F-Actin/G-actin ratios of cells described in (*B*). Bar graphs indicate the quantification (n = 3). $^{*}P < .05$. (*F*) Phalloidin-TRITC and Hoechst 33342 staining in CFPAC-1 cells transfected with scrambled control or miR-802 mimics. Scale bar = 50 μm. (*G*, *H*, *J*, *K*) Expression analysis of 25 predicted miR-802 targets, "PID_RhoA pathway," ductal and acinar markers and the reported "SOX9-regulated genes in pancreas" from the The Cancer Genome Atlas (TCGA) human data set. (*I*) Gene set enrichment analysis highlighting the "Actin Filament Organization" pathway in the same dataset, described in (*G*, *H*, *J*, and *K*). (*L*) Hazard ratios estimated by the Cox proportional hazards model based on the expression of selected genes and overall survival of PDAC patients in the data set from TCGA. Other abbreviations as in Figure 5.

RhoA is a critical regulator of Rock1 and F-actin organization, and increased levels of Rock1/2 have been shown to correlate with reduced survival in PDAC patients.[47] However, upstream regulators of the RhoA–Rock1–F-actin pathway in oncogenic *Kras*-mediated ADM are not well studied. We demonstrated that miR-802 regulates the principle downstream RhoA-related F-actin pathway (Rock1, Limk1, Cofilin1, EZR), as well as F-actin rearrangement in acinar cells bearing the $Kras^{G12D}$ mutation, in well developed human PDAC cells and in biopsies from pancreatic cancer patients. Furthermore, their increased expression levels correlate with poor survival. These findings indicate a supportive role of F-actin organization in pancreatic cancer development and are consistent with the notion that increased F-actin provides protective effects for tumor cells to cope with the compressive stress within solid tumors.[48,49]

In addition to this genetic/biochemical evidence for the role of miR-802 to regulate RhoA activity and the downstream Rock1-Limk1-Cofilin1 pathway as well as F-actin reorganization, we perturbed the pathway pharmacologically with the use of inhibitors targeting the protein kinase Cα–dependent Sdc4, the principal downstream kinase of activated RhoA (Rock1), and F-actin polymerization directly in primary acinar cells of *mir-802*KC mice. All inhibitors reduced the number and size of tubular ductal structures, thereby supporting the relevance of this pathway for ADM in oncogenic stress.

Sox9 is expressed in ductal and centroacinar cells in the normal adult pancreas. Under inflammatory conditions or in the presence of oncogenic *Kras*, Sox9 expression increases and regulates pancreatic epithelial cell identity, affecting epidermal growth factor receptor (EGFR) signaling and thus promoting ADM.[4,50] Rock1 as a principle RhoA effector can directly phosphorylate Sox9 at Ser181 site, which promote Sox9 transcriptional activity in chondrocytes.[38] Whether this active Phos-Sox9 (S181) is also regulated in pancreatic cancer remained elusive. The present study demonstrates that the Phos-Sox9 (S181) is restricted within ADM lesions and that its levels are controlled by miR-802 in KC animals and primary acinar explants but not in established PDAC cells. In line with these findings, we show that EGFR signaling is increased and that genes required for the maintenance of ductal (*Spp1*, *Pkd2*) and acinar (*Bhlha15*, *Rbpjl*) identity are activated and repressed, respectively, in *mir-802*–ablated KC animals. These findings indicate a potential ADM-promoting effect of Phos-SOX9 in pancreatic cancer initiation.

This study identifies miR-802 as a novel negative regulator of an interconnecting genomic circuit controlling RhoA–F-actin rearrangement and Phos-Sox9 (S181) levels both in vivo and in primary acinar 3D explants. This circuit controls the dynamics of F-actin polymerization and the levels of Sox9 activity in acinar cells, thereby highlighting an intrinsic regulatory network that controls ADM formation in the presence of oncogenic *Kras*. Thus, the role of miR-802 regulating F-actin reorganization and acinar identity fills the gap between oncogenic *Kras* signaling and acinar-to-ductal reprogramming underlying pancreatic cancer initiation.

Supplementary Material

Note: To access the supplementary material accompanying this article, visit the online version of *Gastroenterology* at www.gastrojournal.org, and at https://doi.org/10.1053/j.gastro.2021.09.029.

References

1. Rawla P, Sunkara T, Gaduputi V. Epidemiology of pancreatic cancer: global trends, etiology and risk factors. World J Oncol 2019;10:10–27.
2. Storz P, Crawford HC. Carcinogenesis of pancreatic ductal adenocarcinoma. Gastroenterology 2020; 158:2072–2081.
3. Waters AM, Der CJ. KRAS: the critical driver and therapeutic target for pancreatic cancer. Cold Spring Harb Perspect Med 2018;8:a031435.
4. **Kopp JL, von Figura G**, Mayes E, et al. Identification of Sox9-dependent acinar-to-ductal reprogramming as the principal mechanism for initiation of pancreatic ductal adenocarcinoma. Cancer Cell 2012;22:737–750.
5. Storz P. Acinar cell plasticity and development of pancreatic ductal adenocarcinoma. Nat Rev Gastroenterol Hepatol 2017;14:296–304.
6. Tesfaye AA, Azmi AS, Philip PA. miRNA and gene expression in pancreatic ductal adenocarcinoma. Am J Pathol 2019;189:58–70.
7. Wang YJ, McAllister F, Bailey JM, et al. Dicer is required for maintenance of adult pancreatic acinar cell identity and plays a role in Kras-driven pancreatic neoplasia. Plos One 2014;9:e113127.
8. Morris JP, Greer R, Russ HA, et al. Dicer regulates differentiation and viability during mouse pancreatic cancer initiation. Plos One 2014;9:e95486.
9. Sutaria DS, Jiang J, Azevedo-Pouly AC, et al. Knockout of acinar enriched microRNAs in mice promote duct formation but not pancreatic cancer. Sci Rep 2019; 9:11147.
10. Muller S, Raulefs S, Bruns P, et al. Next-generation sequencing reveals novel differentially regulated mRNAs, lncRNAs, miRNAs, sdRNAs and a piRNA in pancreatic cancer (vol 14, 94, 2015). Molecular Cancer 2015;14:94.
11. **Goga A, Yagabasan B, Herrmanns K**, et al. miR-802 regulates Paneth cell function and enterocyte differentiation in the mouse small intestine. Nat Commun 2021; 12:3339.
12. Tuveson DA, Shaw AT, Willis NA, et al. Endogenous oncogenic K-ras(G12D) stimulates proliferation and widespread neoplastic and developmental defects. Cancer Cell 2004;5:375–387.
13. Kawaguchi Y, Cooper B, Gannon M, et al. The role of the transcriptional regulator Ptf1a in converting intestinal to pancreatic progenitors. Nat Genet 2002;32:128–134.
14. Kopinke D, Brailsford M, Pan FC, et al. Ongoing Notch signaling maintains phenotypic fidelity in the adult exocrine pancreas. Dev Biol 2012;362:57–64.

15. **Olive KP, Tuveson DA**, Ruhe ZC, et al. Mutant p53 gain of function in two mouse models of Li-Fraumeni syndrome. Cell 2004;119:847–860.
16. Dixit AK, Sarver AE, Yuan ZB, et al. Comprehensive analysis of microRNA signature of mouse pancreatic acini: overexpression of miR-21-3p in acute pancreatitis. Am J Physiol Gastrointest Liver Physiol 2016; 311:G974–G980.
17. Guerra C, Schuhmacher AJ, Canamero M, et al. Chronic pancreatitis is essential for induction of pancreatic ductal adenocarcinorna by k-Ras Oncogenes in adult mice. Cancer Cell 2007;11:291–302.
18. Reichert M, Rustgi AK. Pancreatic ductal cells in development, regeneration, and neoplasia. J Clin Invest 2011; 121:4572–4578.
19. Lesina M, Kurkowski MU, Ludes K, et al. Stat3/Socs3 activation by IL-6 transsignaling promotes progression of pancreatic intraepithelial neoplasia and development of pancreatic cancer. Cancer Cell 2011;19:456–469.
20. Guerra C, Collado M, Navas C, et al. Pancreatitis-induced inflammation contributes to pancreatic cancer by inhibiting oncogene-induced senescence. Cancer Cell 2011;19:728–739.
21. Gruber R, Panayiotou R, Nye E, et al. YAP1 and TAZ control pancreatic cancer initiation in mice by direct up-regulation of JAK-STAT3 signaling. Gastroenterology 2016;151:526–539.
22. Zhou YY, Zhou B, Pache L, et al. Metascape provides a biologist-oriented resource for the analysis of systems-level datasets. Nat Commun 2019;10:1523.
23. Hodge RG, Ridley AJ. Regulating Rho GTPases and their regulators. Nat Rev Mol Cell Biol 2016;17:496–510.
24. Dovas A, Yoneda A, Couchman JR. PKCβ-dependent activation of RhoA by syndecan-4 during focal adhesion formation. J Cell Sci 2006;119:2837–2846.
25. **Row S, Liu Y**, Alimperti S, et al. Cadherin-11 is a novel regulator of extracellular matrix synthesis and tissue mechanics. J Cell Sci 2016;129:2950–2961.
26. Quilliam LA, Lambert QT, MickelsonYoung LA, et al. Isolation of a NCK-associated kinase, PRK2, an SH3-binding protein and potential effector of Rho protein signaling. J Biol Chem 1996;271:28772–28776.
27. Krebs AM, Mitschke J, Lasierra Losada M, et al. The EMT-activator Zeb1 is a key factor for cell plasticity and promotes metastasis in pancreatic cancer. Nat Cell Biol 2017;19:518–529.
28. Zhang Y, Morris JPt, Yan W, et al. Canonical Wnt signaling is required for pancreatic carcinogenesis. Cancer Res 2013;73:4909–4922.
29. Nakano K, Kanai-Azuma M, Kanai Y, et al. Cofilin phosphorylation and actin polymerization by NRK/NESK, a member of the germinal center kinase family. Exp Cell Res 2003;287:219–227.
30. Rath N, Olson MF. Rho-associated kinases in tumorigenesis: re-considering ROCK inhibition for cancer therapy. EMBO Rep 2012;13:900–908.
31. Hebert M, Potin S, Sebbagh M, et al. Rho-ROCK–dependent Ezrin-Radixin-Moesin phosphorylation regulates Fas-mediated apoptosis in jurkat cells. J Immunol 2008;181:5963–5973.
32. Heid I, Lubeseder-Martellato C, Sipos B, et al. Early requirement of Rac1 in a mouse model of pancreatic cancer. Gastroenterology 2011;141:719–730; e1–7.
33. Nemoto T, Kojima T, Oshima A, et al. Stabilization of exocytosis by dynamic F-actin coating of zymogen granules in pancreatic acini. J Biol Chem 2004; 279:37544–37550.
34. Tao XF, Chen Q, Li N, et al. Serotonin-RhoA/ROCK axis promotes acinar-to-ductal metaplasia in caerulein-induced chronic pancreatitis. Biomed Pharmacother 2020;125:109999.
35. Li F, Higgs HN. The mouse Formin mDia1 is a potent actin nucleation factor regulated by autoinhibition. Curr Biol 2003;13:1335–1340.
36. Ren L, Hong SH, Cassavaugh J, et al. The actin-cytoskeleton linker protein ezrin is regulated during osteosarcoma metastasis by PKC. Oncogene 2009;28:792–802.
37. Parisiadou L, Xie CS, Cho HJ, et al. Phosphorylation of Ezrin/Radixin/Moesin proteins by LRRK2 promotes the rearrangement of actin cytoskeleton in neuronal morphogenesis. Journal of Neuroscience 2009; 29:13971–13980.
38. Haudenschild DR, Chen J, Pang N, et al. Rho kinase–dependent activation of SOX9 in chondrocytes. Arthritis Rheum 2010;62:191–200.
39. Shih HP, Kopp JL, Sandhu M, et al. A Notch-dependent molecular circuitry initiates pancreatic endocrine and ductal cell differentiation. Development 2012; 139:2488–2499.
40. Shang X, Marchioni F, Evelyn CR, et al. Small-molecule inhibitors targeting G-protein–coupled Rho guanine nucleotide exchange factors. Proc Natl Acad Sci U S A 2013;110:3155–3160.
41. Cancer Genome Atlas Research Network. Integrated genomic characterization of pancreatic ductal adenocarcinoma. Cancer Cell 2017;32:185–203.e13.
42. Schaefer CF, Anthony K, Krupa S, et al. PID: the Pathway Interaction Database. Nucleic Acids Res 2009; 37:D674–D679.
43. Zhao Y, Schoeps B, Yao D, et al. mTORC1 and mTORC2 converge on the Arp2/3 complex to promote Kras^{G12D}-induced acinar-to-ductal metaplasia and early pancreatic carcinogenesis. Gastroenterology 2020;160:1755–1770.e17.
44. Valencia K, Erice O, Kostyrko K, et al. The Mir181ab1 cluster promotes KRAS-driven oncogenesis and progression in lung and pancreas. J Clin Invest 2020; 130:1879–1895.
45. Timpson P, McGhee EJ, Morton JP, et al. Spatial regulation of RhoA activity during pancreatic cancer cell invasion driven by mutant p53. Cancer Res 2011; 71:747–757.
46. Cerami E, Gao JJ, Dogrusoz U, et al. The cBio Cancer Genomics Portal: an open platform for exploring multidimensional cancer genomics data. Cancer Discov 2012; 2:401–404.
47. Rath N, Morton JP, Julian L, et al. ROCK signaling promotes collagen remodeling to facilitate invasive pancreatic ductal adenocarcinoma tumor cell growth. EMBO Mol Med 2017;9:198–218.

48. McGrail DJ, McAndrews KM, Brandenburg CP, et al. Osmotic regulation is required for cancer cell survival under solid stress. Biophys J 2015;109:1334–1337.
49. Fletcher DA, Mullins D. Cell mechanics and the cytoskeleton. Nature 2010;463:485–492.
50. Grimont A, Pinho AV, Cowley MJ, et al. SOX9 regulates ERBB signalling in pancreatic cancer development. Gut 2015;64:1790–1799.

Author names in bold designate shared co-first authorship.

Received May 6, 2021. Accepted September 14, 2021.

Correspondence
Address correspondence to: Markus Stoffel, ETH Zurich, Institute of Molecular Health Sciences, HPL H36, Otto-Stern-Weg 7, 8093 Zürich, Switzerland. e-mail: stoffel@biol.ethz.ch.

Acknowledgments
The authors thank R. Kubsch, H. Kabakci, G. Tang, J. Xue, Y. Yang, L. Hasenöhrl, A.C. Title, M. LaPierre, F. Villena, H. Vatandaslar, Y. Büsra, N. Frey, and K.K. Tu for their advice. The authors thank the Functional Genomics Center Zurich for RNA sequencing, the Flow Cytometry Core Facility of the Swiss Federal Institute of Technology in Zurich for fluorescence-activated cell sorting, and the Scientific Center for Optical and Electron Microscopy for support.

CRedit Authorship Contributions
Wenjie Ge, PhD (Conceptualization: Equal; Investigation: Lead; Data curation: Lead; Formal analysis: Lead; Validation: Lead; Visualization: Lead; Methodology: Lead; Writing-original draft: Lead; Writing-review & editing: lead); Algera Goga (Investigation: Supporting; Data curation: Supporting; Methodology: Supporting; Resources: Supporting; Writing-original draft: Supporting); Yuliang He (Data curation: Supporting; Visualization: Supporting; Software: Equal; Visualization: Equal; Formal analysis: Supporting; Writing-original draft: Supporting; Writing-review & editing: Supporting); Pamuditha N. Silva, PhD (Investigation: Supporting; Data curation: Supporting; Methodology: Supporting); Christian Kurt Hirt, MD, PhD (Investigation: Supporting; Data curation: Supporting; Methodology: Supporting; Writing-original draft: Supporting; Funding acquisition: Supporting); Karolin Herrmanns, PhD (Investigation: Supporting; Data curation: Supporting; Methodology: Supporting); Ilaria Guccini, PhD (Methodology: Supporting; Resources: Supporting); Svenja Godbersen (Investigation: Supporting; Data curation: Supporting; Methodology: Supporting; Resources: Supporting); Gerald Schwank, PhD (Resources: Equal); Markus Stoffel, MD, PhD (Conceptualization: Lead; Funding acquisition: Lead; Supervision: Lead; Project administration: Lead; Writing-original draft: Lead; Writing-review & editing: lead).

Conflicts of interest
The authors declare no conflicts.

Funding
This project was funded in part by the Swiss National Science Foundation (310030_176317). Christian Kurt Hirt holds a transition postdoctoral fellowship from the Personalized Health and Related Technology Initiative of the Swiss Federal Institute of Technology (2018-423).

Data Transparency
The RNA-seq raw data was deposited at the European Nucleotide Archive with the study accession number E-MTAB-10411. Further information and requests for resources and reagents should be directed to and will be fulfilled by the corresponding author, Markus Stoffel (stoffel@biol.ethz.ch).